

Linear viscoelasticity of PP/PS/MWCNT composites with co-continuous morphology

Daria Strugova, Éric David and Nicole R. Demarquette *

Mechanical Engineering Department, École de Technologie Supérieure, Montréal, Québec H3C 1K3, Canada;

* Correspondence: NicoleR.Demarquette@etsmtl.ca

Abstract

In this work, a study of the linear viscoelastic properties of co-continuous polypropylene/polystyrene (PP/PS) blends filled with multi-wall carbon nanotubes (MWCNT) is presented. The YZZ rheological model [1] is employed to correlate the rheological behavior of the blends with their microstructure and electrical properties. A test design involving a sequence of small amplitude oscillatory shear (SAOS) and a time sweep (simulating thermal annealing) is used to evaluate the morphology and electrical properties evolution. It was shown that the YZZ rheological model could be successfully modified to be able to quantify a co-continuous morphology of filled composites. The calculated characteristic domain size was found to be in good agreement with the experimental data obtained via scanning electron microscopy (SEM). Furthermore, it is shown that the characteristic domain size slightly decreased after 30 min of thermal annealing. It was shown, as well, that, thermal annealing promoted a reduction of the electrical percolation threshold (wt.% MWCNT) from 0.28 to 0.06.

I. INTRODUCTION

Over the last few years, it has been shown that through proper processing, the morphology of a blend to which nanoparticles are added, can be manipulated to achieve satisfactory engineering properties. For example, it has been shown that the use of nanostructured blends [2-5] or block copolymers [6-8] can help in tailoring the location and orientation of nanoparticles affecting properties such as electrical conductivity [9-11], electromagnetic interference shielding [2,3], dielectric properties [5], and thermal properties among others. In particular, it has been shown that the electrical percolation threshold of carbonaceous nanoparticles composites could be greatly reduced by using the so-called double percolation technique which consists of tailoring the location of a conductive filler in one of the components or the interface between both polymers, forming a blend with a co-continuous morphology [9,11-13].

However, during processing, such composites are subjected to further deformation which could result in a change of their morphology. Rheological tests may be used to probe such an evolution [14,15]. Indeed, small amplitude oscillatory shear (SAOS) tests carried out in the linear viscoelastic region can be used to characterize the equilibrium morphology of binary blends [16-22]. Therefore, if a blend is subjected to SAOS – deformation – SAOS, a second SAOS test after deformation will indicate, to some extent, if the morphology of the blend will have evolved during that deformation. Rigorously, SAOS can only be used to access equilibrium morphology, and whether or not a highly nonlinear deformation, the morphology will not have reached equilibrium. A more accurate test would be SAOS – deformation – recovery – SAOS. SAOS – deformation – SAOS has been extensively used for dispersed droplet type polymer blends [23-27] as their

rheological behavior in SAOS is well described by the well-known Palierne [16], Gramespacher and Meissner [17], or Bousmina [18] models. However, to our knowledge, such an analysis is scarce in the case of co-continuous morphology type blends. Proper models relating the rheological behavior of the blend to its co-continuous morphology, quantitatively, are still being developed [1,6,28]. Indeed, several models have been developed to predict the rheological behavior of polymer blends with a co-continuous morphology [1,6,28-31], however, only a few allow a quantitative evaluation of the morphology from the rheological analysis.

One such model is that developed by Yu et al. [1], referred to as the YZZ model in the present manuscript, as well as in their later article [32]. It is based on the basic idea that the complex modulus of a blend $G_{blend}^*(\omega)$ with a co-continuous morphology can be evaluated as the sum of both components' contribution, symbolized by $G_{components}^*(\omega)$, and an interface contribution symbolized by $G_{interface}^*(\omega)$ resulting in [16,17]:

$$G_{blend}^*(\omega) = G_{components}^*(\omega) + G_{interface}^*(\omega) \quad (1)$$

To calculate the contribution of the components, Yu et al. [1] adapted the expression, developed by Veenstra et al. [33], to evaluate the complex and/or storage moduli of a blend with co-continuous morphology. In the present manuscript, both components and interface contributions are used for the storage modulus of a blend with a co-continuous morphology. In their model, Veenstra et al. [33] assumed, that the microstructure of the blend with a co-continuous morphology is schematically shown in Figure 1(a). An elementary cell of a co-continuous microstructure is 1/8 of the primary microstructure and is assumed to consist of three connected parallelepiped shape elements of length $l'_c = a' + b' = 1$, square section of edge a' , and $b' = 1 - a'$ as shown in Figure 1(b). If the length of the cell is normalized to 1, and φ_1 is the volume fraction of fluid 1, as shown in Figure 1(c), then φ_1 amounts to:

$$\varphi_1 = 3a'^2 - 2a'^3 \quad (2)$$

Using these geometrical assumptions, the storage modulus of the blend can then be written as:

$$G'_{components} = \frac{a'^2 b' G_1'^2(\omega) + (a'^3 + 2a' b' + b'^3) G_1'(\omega) G_2'(\omega) + a' b'^2 G_2'^2(\omega)}{b' G_1'(\omega) + a' G_2'(\omega)} \quad (3)$$

Where $G_1'(\omega)$ is the storage modulus of component 1; $G_2'(\omega)$ is the storage modulus of component 2.

To evaluate the contribution of the interface, Yu et al. [1] modified the scheme of Veenstra et al. [33] by considering that the parallelepiped shape elements should be in fact cylinders to take into account the minimization of the surface area (see Figure 1(c)). These cylinders are assumed to have a radius a and a characteristic length l_c with $a' = a/l_c$ and $b' = b/l_c$. Then, they calculated the stress contribution induced by the interfacial deformation of each cylinder. This results in expression (4) for the storage modulus of the interface contribution as:

$$G'_{interface} = G_A'_{interface} + G_B'_{interface} + G_C'_{interface} \quad (4)$$

Where $G_A' interface$, $G_B' interface$, $G_C' interface$ are the elastic moduli due to interface deformation of the cylinder type A, type B and type C, respectively.

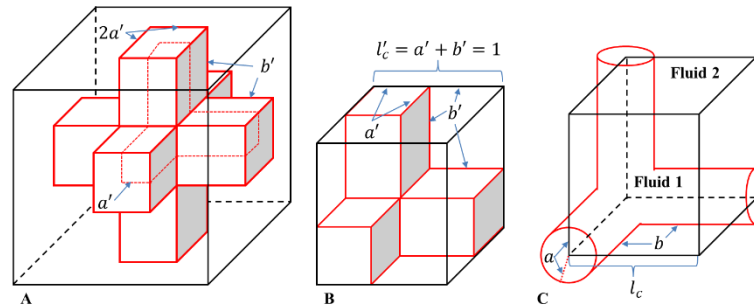


Figure 1. A schematic of an ideal co-continuous morphology (redrawn from ref. [1,33]).

In doing so they were able to derive an expression for $G' interface$ as:

$$G' interface = \frac{k_C}{6} \alpha S_V \left(\frac{k_B}{k_C} + \frac{3}{4} \frac{f_2 \omega^2 \tau^2}{f_1^2 + \omega^2 \tau^2} \right) \quad (5)$$

where α is the interfacial tension, ω is the frequency, S_V is the specific area, inversely proportional to the characteristic domain size ξ , given by:

$$S_V = \frac{3\pi ab}{2l_c^3} = \frac{1}{\xi} \quad (5a)$$

$$\tau = \frac{\eta_m a}{\alpha} \quad (5b)$$

$$k_C = -\frac{f_2 \omega^2 \tau^2}{f_1^2 + \omega^2 \tau^2} \gamma_0 \quad (5c)$$

$$k_B = -\frac{f_1 f_2 \omega \tau}{f_1^2 + \omega^2 \tau^2} \gamma_0 \quad (5d)$$

with

$$f_1 = \frac{40(p+1)}{(2p+3)(19p+16)} \quad (5e)$$

and

$$f_2 = \frac{5}{2p+3} \quad (5f)$$

where p is the viscosity ratio of fluid 1 over fluid 2, and γ_0 is the strain amplitude. k_B and k_C are constants that relate to a random orientation and possible distortion of a co-continuous element, and the ratio $k_B/k_C \leq 1$.

Using equation (2) and (5) the storage modulus of the blend with a co-continuous morphology can be written as:

$$G'_{blend}(\omega) = \frac{a'^2 b' G_1'^2(\omega) + (a'^3 + 2a' b' + b'^3) G_1'(\omega) G_2'(\omega) + a' b'^2 G_2'^2(\omega)}{b' G_1'(\omega) + a' G_2'(\omega)} \quad (6)$$

$$+ \frac{k_C}{6} \alpha S_V \left(\frac{k_B}{k_C} + \frac{3}{4} \frac{f_2 \omega^2 \tau^2}{f_1^2 + \omega^2 \tau^2} \right)$$

where G_1' is the storage modulus of component 1; G_2' is the storage modulus of component 2;

More details can be found in Yu et al. work [1].

However, in the case of the YZZ model, the linear viscoelastic properties are well described just for neat polymer blends with a co-continuous morphology. In the case of blends to which nanoparticles are added, the elastic contribution from the filler network has a significant effect on the elastic modulus of the composite, which was widely observed for different polymer blend/filler systems [6,10,34]. As a result, it can be concluded that the influence of a rigid filler network in the modeling of viscoelastic properties of a co-continuous morphology of polymer blends requires further investigation. Such a tool would enable the study of the stability of a co-continuous blend morphology to which nanoparticles are added, as well as, of the stability of their electrical properties. Indeed, with such a model it would be possible to use the response of co-continuous filled nanocomposites subjected to SAOS – deformation – SAOS to evaluate the effect of deformation on their morphology.

In particular, it was shown, in our previous work [9], that it is possible to achieve an electrical percolation threshold using ultra-low values of MWCNT concentrations in PP/PS/MWCNT composites. This ultra-low percolation threshold concentration is achieved by applying thermal treatment that affect PP crystal growth. However, it is very important to study the stability of the obtained morphologies to avoid loss of properties (in particular electrical conductivity) during further processing.

In the present manuscript, the YZZ model was modified for systems containing nanoparticles and used to evaluate the effect of thermal annealing on the morphology of the PP/PS/MWCNT composites studied in our previous work.

II. MATERIALS AND METHODS

A. Materials

PP, grade PP4712E1, from Exxon Mobile and PS, grade MC3650, from PolyOne were used in this work. The characteristics of these polymers are reported in Table 1. MWCNT, grade NC7000TM, were purchased from Nanocyl. The nanotubes have an average diameter of 9.5 nm and a length of 1.5 μm with a nominal electrical conductivity of $10^6 \text{ S}\cdot\text{m}^{-1}$.

Table 1. Properties of the polymers.

Polymers	Melt index	η_0 (Pa·s) at 200 °C	Density (g·cm ⁻³)
PP	2.8 g/10 min (230°C/2.16kg)	7800	0.9
PS	13 g/10 min (200°C/5kg)	4080	1.04

B. Composites preparation

All composites were prepared by melt-mixing process using a Haake Rheomix OS PTW16 twin-screw extruder (Thermo Fisher Scientific Inc., Waltham, MA, USA). The temperature was fixed at 220 °C in all zones, and the screw speed was adjusted to 100 rpm for all compositions. First, a masterbatch of PP with 10 wt.% of MWCNT was prepared. Second, PP/PS/MWCNT composites with a MWCNT concentration varying from 0 to 2 wt.% were prepared by diluting the PP/MWCNT masterbatch with PP and PS to the concentration of PP/PS of 50/50 wt.% where a co-continuous morphology was obtained.

A 50/50 wt.% PP/PS concentration was chosen as it would yield a co-continuous morphology based on the analysis of Jordhamo et al. [35], as was explained in our previous work [9].

Samples for rheological, electrical, and morphological analyses were obtained by compression molding. Disks with a 25 mm diameter and 1 mm thickness were molded at 200 °C under 0.8 MPa for 10 min, after that, the pressure was increased to 10 MPa, and samples were molded for additional 10 min at the reached pressure.

C. Characterizations

Rheology

The rheological characterization of all composites was performed using a controlled-stress MCR 501 rotational rheometer (Anton Paar, Graz, Austria). Measurements were carried out under a dry nitrogen atmosphere. A parallel-plate geometry was used with a gap size of 1 mm and a plate diameter of 25 mm. All tests were carried out at 200 °C. First, dynamic strain sweep tests (DSST) were performed for all composites at three different angular frequencies, 1, 10, and 100 rad/s, in a strain range from 0.01 to 10 % in order to determine the linear viscoelastic region. A strain of 0.3% was chosen as it was found to correspond to the LVE region, for all composites in the studied range. Second, time sweep tests were performed for pure PP and PS at 0.05 rad/s for 6 h at the fixed strain of 0.3 % in order to check the thermal stability of the samples. Then, small amplitude oscillatory shear (SAOS) tests were performed with frequencies ranging from 300 to 0.01 1/s at a fixed strain of 0.3 % for all composites. For each composite, a sequence of SAOS, followed by a time sweep (simulating thermal annealing), followed by another SAOS, as shown in Figure 2, was carried out to evaluate the evolution of morphology during thermal annealing. This sequence can be used whether or not an equilibrium morphology is reached after annealing.

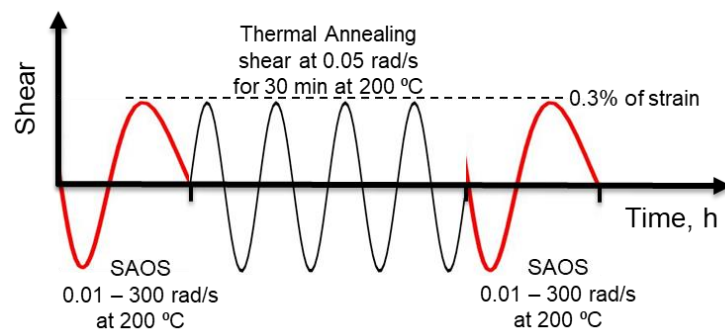


Figure 2. Experimental protocol.

Electrical conductivity

Combined rheological and electrical characterization of the PP/PS/MWCNT composites, was carried out during the middle time step, using the MCR501 rheometer equipped with a dielectrorheological device (DRD with ST2826/A high-frequency LCR meter). The time sweep was carried out at an angular frequency equal to 0.05 rad/s. Measurements of electrical properties were performed by applying 20 Hz AC of 1 V_{RMS} across the sample.

The electrical conductivity at 200 °C (see Figure 7(a) in Results and Discussion section) was evaluated from the complex impedance using:

$$\sigma' = \frac{1}{Z'} \frac{d}{A} \quad (7)$$

where Z' is the real part of the complex impedance, A is the plate area, and d is the distance between the plates.

At room temperature the electrical conductivity of the obtained composites was rather characterized using a broadband dielectric spectrometer (BDS) (Novocontrol Technologies GmbH & Co. KG, Montabaur, Germany). The measurements were conducted in a frequency range from 10^{-2} to 3×10^5 Hz under an excitation voltage of 1 V_{RMS} applied across the sample. The calculation of the electrical conductivity from the complex capacitance has been explained in detail in our previous work [9]. The electrical conductivity values, presented in the Results and Discussion section using this device, refer to the value of $\sigma'(\omega)$ at a frequency of 10^{-2} Hz. Disks of 25 mm in diameter and 1 mm in thickness, covered on both sides with 20 nm of gold, serving as electrodes, were used for the measurements.

Microscopy analysis

The morphology of PP/PS/MWCNT composites was observed by scanning electron microscopy (SEM) using a S3600 Hitachi microscope (Hitachi, Ltd., Tokyo, Japan), operated at 5 kV in the secondary electrons' mode. The samples were fractured in liquid nitrogen and then the polystyrene

was extracted by using butanone at room temperature, under continuous stirring for two hours. Then, the samples were dried under vacuum at room temperature for 12 h. After drying, the samples were covered with gold using a gold sputter coater, model K550X.

The state of dispersion and localization of MWCNT in PP/PS/MWCNT composites before and after thermal annealing was evaluated by transmission electron microscopy (TEM). To obtain 50–100 nm ultrathin sections, the investigated samples were embedded in epoxy resin, and the sectioning was performed using a Leica Microsystems UC7/FC7 cryoultramicrotome operated at -160 °C. Imaging was carried out with a Thermo Scientific Talos F200X G2 S/TEM at an accelerating voltage of 200 kV.

III. RESULTS AND DISCUSSION

As mentioned in the introduction, our previous study had shown that it is possible to obtain electrically conductive PP/PS/MWCNT composites with ultra-low percolation threshold concentrations of 0.06 wt.% and 0.08wt% of MWCNT after applying thermal treatments. These thermal treatments had the benefit of resulting in a decrease of percolation threshold concentration without affecting the overall blend morphology. The aim of this work is to study the stability of the morphologies obtained. For that, a method to characterize the composites morphology from their rheological behavior needed to be developed. This is what is described in part A of this result section. Then, the tool is used to study the systems after thermal annealing to explain the evolution of their electrical and morphological properties during thermal annealing.

A. PP/PS/MWCNT composites morphology and the YZZ model fitting

Figure 3 shows the storage modulus as a function of frequency for pure PP, PS, PP/PS blend of 50/50 wt.% and PP/PS/MWCNT (50/50/x wt.%) composites with different concentrations of MWCNT. It can be seen that the experimentally obtained storage modulus of the blend, at low frequencies, is higher than the ones for the pure components. The reason for the increase of G' for polymer blends originates from an extra contribution of the stress generated by the deformation of the interface [17]. It can be also seen that the storage modulus at low frequencies increases with MWCNT concentration, exhibiting a plateau what indicates a solid-like behavior due to the formation of a rigid nanoparticles network [10,20,34]. Concomitantly, it has been shown that independently of the complexity of the filled composite's matrix, the filler network contributes more to the elastic modulus at low frequencies with frequency-independent elastic modulus – G'_0 compared to the matrix response [36-38].

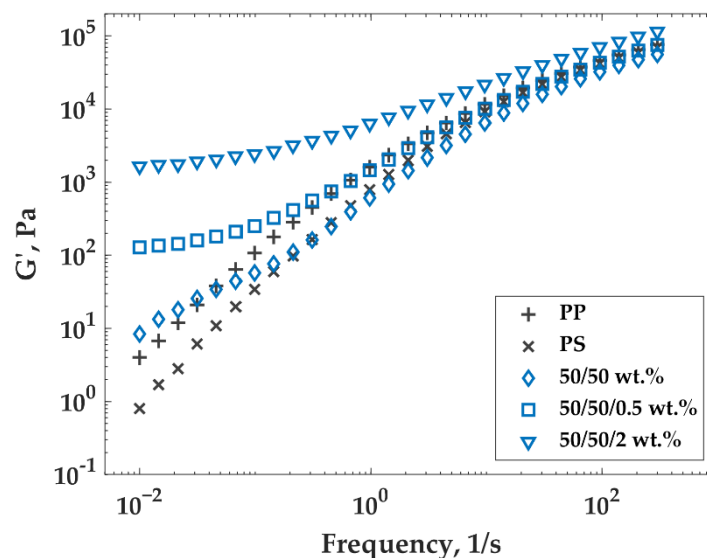


Figure 3. Storage modulus as a function of frequency for PP/PS/MWCNT composites with different concentrations of MWCNT at 200 °C. PP, PS, PP/PS blend of 50/50 wt.%

Figure 4 shows the rheological behavior of PP/PS 50/50 wt.% blend with the YZZ model fitting (Figure 4(a)) and PP/PS blend to which 0.3wt.% of MWCNT (Figure 4(b)) was added with the YZZ model fitting. The dashed line in both graphs shows the fit of the YZZ model. The data for storage and loss moduli as a function of frequency for PP/PS/MWCNT (50/50/x wt.%) composites for all concentrations of MWCNT are reported in Figure S1(a-b) of the supplementary material.

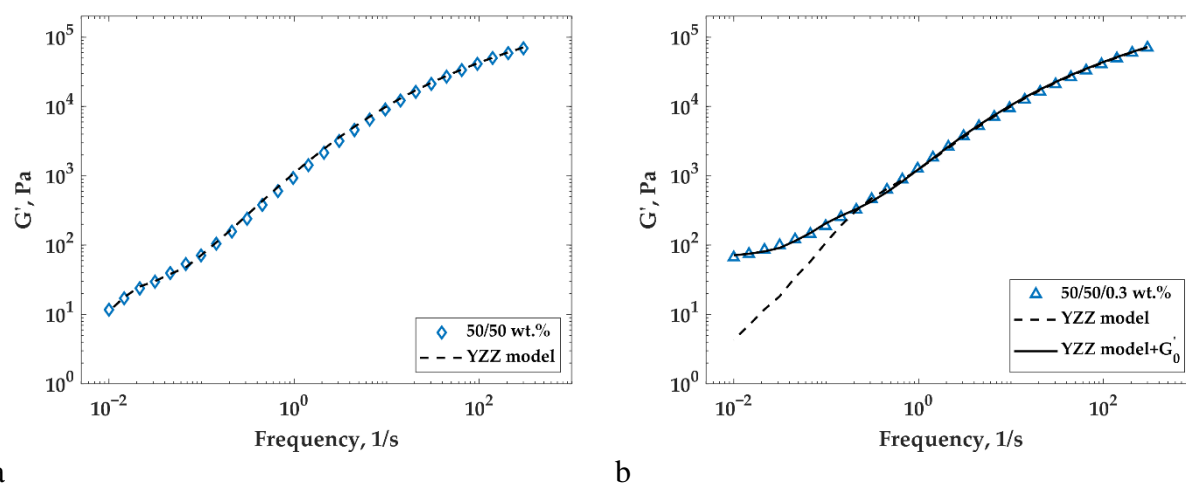


Figure 4. Storage modulus as a function of frequency for: a) PP, PS and PP/PS blend with YZZ model fitting data (dashed line) and b) PP/PS/MWCNT composite with 0.3 wt.% of MWCNT with model data representing the fit of YZZ model (dashed line) and model data representing the fit of the Equation (9) (solid line).

It can be seen that the YZZ model describes well the experimental data in the absence of MWCNT. It should be noted that fitting the model to the experimental data requires knowledge of the value of the zero-shear viscosity ratio (η_0) and interfacial tension. Zero shear viscosity of neat PP and

PS was found by fitting the experimental data to the Carreau model [39,40], using the curve of complex viscosity (Pa·s) versus frequency (rad/s), obtained from SAOS tests. The values of η_0 are presented in Table 1. The value for interfacial tension was taken from the literature [41]. Using a viscosity ratio of 0.52 and an interfacial tension of 6 mN/m, fitting the YZZ model to the experimental data resulted in an a value of 4.95 μm . $l_c = a/a'$ was then found to be 10.45 μm . These values were used in Equation (5a) to obtain the value of $\xi = 8.9 \mu\text{m}$ for the neat blend. This corroborates rather well with the morphological characterization, presented in Figure 5(a), in which a value of $\xi = 11 \pm 0.8 \mu\text{m}$ was found using Equation (8) [10,42]:

$$\xi = \frac{A_{SEM}}{L_{int}} \quad (8)$$

where A_{SEM} is the total area of the SEM micrograph (Figure 5), and L_{int} is the interface length, estimated using a homemade image analysis script (written in MATLAB). (Note that these analyses were done for at least 7 images). The MATLAB code for SEM pictures treatment and calculation of the perimeter of the interface (interfacial length) was written based on the analysis described by Galloway et al. [43]. The steps of image treatment for interface indication are shown in Figure S3(a-b) of the supplementary material.

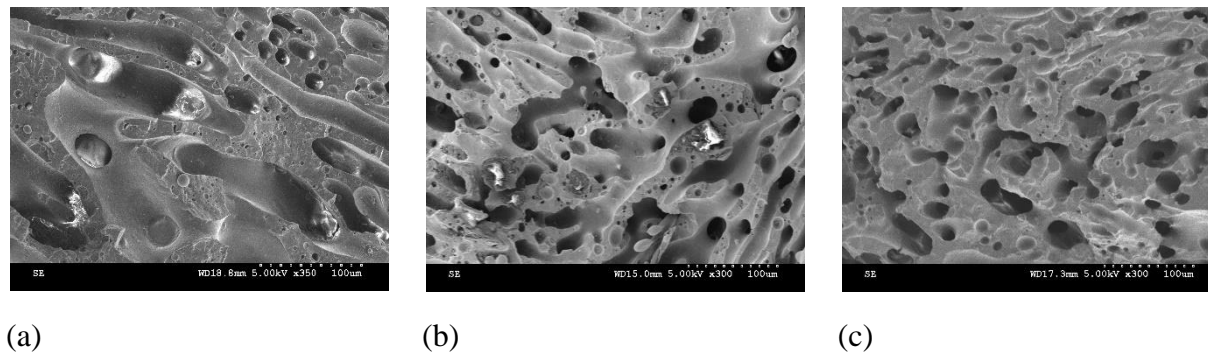


Figure 5. Morphology evolution of selected PP/PS/MWCNT composites for: (a) 0 wt.% of MWCNT; (b) 0.3 wt.% of MWCNT; and (c) 0.5 wt.% of MWCNT.

Figure 4(b) shows, that the YZZ model fails to describe the rheological behavior at lower frequencies for PP/PS/MWCNT composite containing 0.3 wt.% MWCNT independently of the value of a used. This was observed for all PP/PS/MWCNT composites. The discrepancy between the experimental values of G' and the ones predicted by the model was much larger at low frequencies. One way to deal with this discrepancy is to add, as was done in this work, a frequency-independent elastic modulus, G'_0 , to the YZZ model resulting in:

$$G'_{blend}(\omega) = G'_{components}(\omega) + G'_{interface}(\omega) + G'_0 \quad (9)$$

where G'_0 is a constant that takes into account the filler network elasticity.

Using Equation (9) it was then possible to achieve a good fit of storage modulus for all PP/PS/MWCNT composites. Two fitting parameters were found when adjusting Equation (9) to the experimental data: a and G'_0 . Figure 4(b) shows the result of this fit (solid line) for PP/PS/MWCNT with 0.3 wt.% of MWCNT. In this case, the values of G'_0 of 66.2 Pa and a of 1.18

μm were resulted in a value of $\xi = 2.13 \mu\text{m}$ which agrees well with the morphological characterization of Figure 5(b) for which a value of $\xi = 1.86 \pm 0.2 \mu\text{m}$ was found.

Equation (9) was tested as a tool to quantify the morphology of the different composites studied in this work using the data presented in Figure S1 of the supplementary material (model fitting results for all composites are shown in Figure S2 of the supplementary material). A comparison of the characteristic domain size evaluated using the morphological and rheological data is presented in Figure 6. It can be seen that a good agreement was obtained for all composites. The larger discrepancy obtained for the neat blend, probably, originated from the non-fully developed co-continuous morphology which was observed for the neat blend.

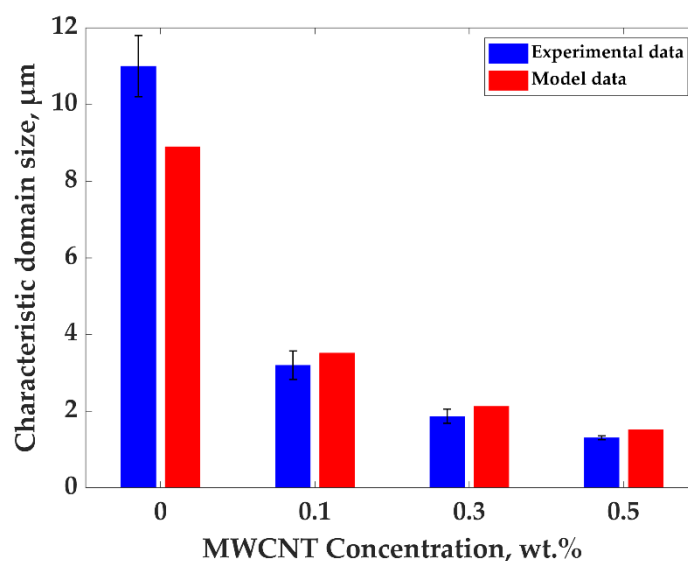


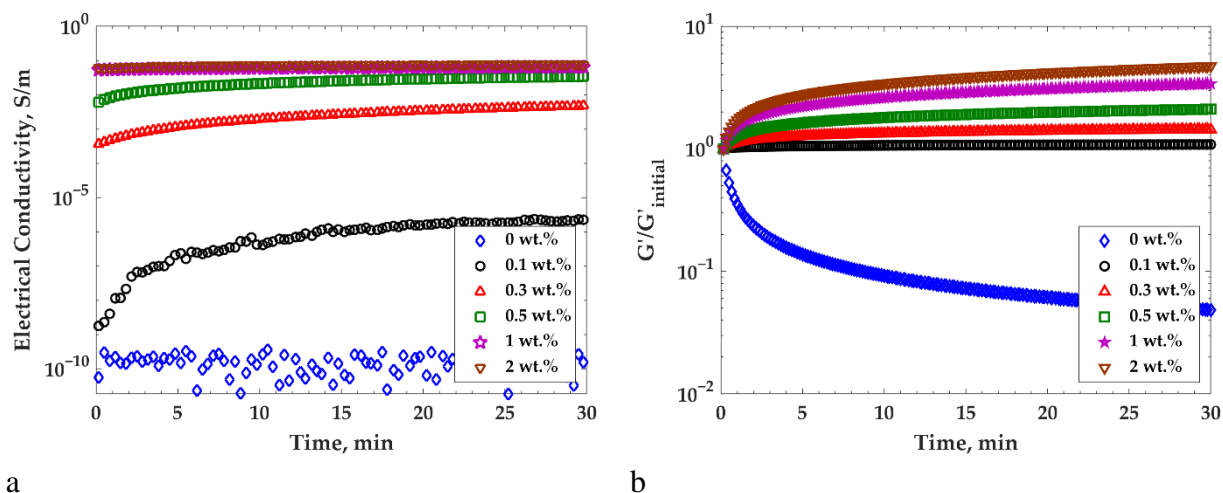
Figure 6. Characteristic domain size of PP/PS/MWCNT composites calculated with the help of Equation (7) – experimental data and predicted with the YZZ model for PP/PS/MWCNT with 0-0.1 wt.% of MWCNT and the Equation (9) for PP/PS/MWCNT with 0.3-0.5 wt.% of MWCNT – model data.

It can also be seen that the characteristic domain size drastically decreases from 11 ± 0.8 to $1.3 \pm 0.05 \mu\text{m}$ upon the addition of 0.5 wt.% of MWCNT. A drastic decrease of the characteristic domain size was observed, in the literature, for different blend systems filled with carbon-based nanoparticles, as their presence helps to prevent the coalescence and coarsening of the blend morphology [6,9,42,44].

B. Effect of thermal annealing on electrical conductivity and characteristic domain size of co-continuous morphology of PP/PS/MWCNT composites

The PP/PS/MWCNT composites morphology evolution during thermal annealing was investigated using the experimental protocol presented in Figure 2. Figure 7 shows the electrical and rheological behavior of PP/PS/MWCNT composites during the middle step – time sweep (simulating thermal annealing, see Figure 2). Figure 7(a) shows the electrical conductivity of PP/PS/MWCNT composites as a function of time during the thermal annealing, performed using the rheometer

connected with the DRD cell. Figure 7(b) shows the time-dependent evolution of the storage modulus for PP/PS/MWCNT composites.



a b
Figure 7. (a) Electrical conductivity as a function of time for PP/PS/MWCNT composites with different concentrations of MWCNT measured at 20 Hz of frequency and 200 °C. (b) Time-dependent evolution of storage modulus at 200 °C for PP/PS/MWCNT composites with different MWCNT concentration.

It can be seen, from Figure 7(a), that even at a very low concentration of MWCNT the electrical conductivity starts to increase from the first seconds and reaches a plateau. The increase could originate from a MWCNT nanoparticles network formation during thermal annealing. Similar behavior was observed by other authors for different polymer pairs such as PaMSAN/PMMA with MWCNT [45], and for PLA/PS filled with reduced graphene oxide [6]. However, in those cases the authors observed electrical conductivity increase only for a large MWCNT concentration and/or after long annealing times. After thermal annealing a low value of electrical percolation threshold (PT) was reached. This happened due to double percolation effect [13,42,46] and due to the destruction of the filler agglomerates and reformation of the electrically conductive network [47] which both reduce the electrical PT. In order to confirm the localization of MWCNT in PP/PS/MWCNT composites before and after thermal annealing, TEM was performed for PP/PS/MWCNT composite with 0.5 wt.% of MWCNT. Figure 8 (a) and 8(b) show the images corresponding to PP/PS/MWCNT composite with 0.5 wt.% of MWCNT before thermal annealing and Figure 8 (c) and 8(d) show the images corresponding to the same composite after thermal annealing. It was observed that for PP/PS/MWCNT composite with 0.5 wt.% of MWCNT after thermal annealing, the nanoparticles are mostly located at the PP/PS interface.

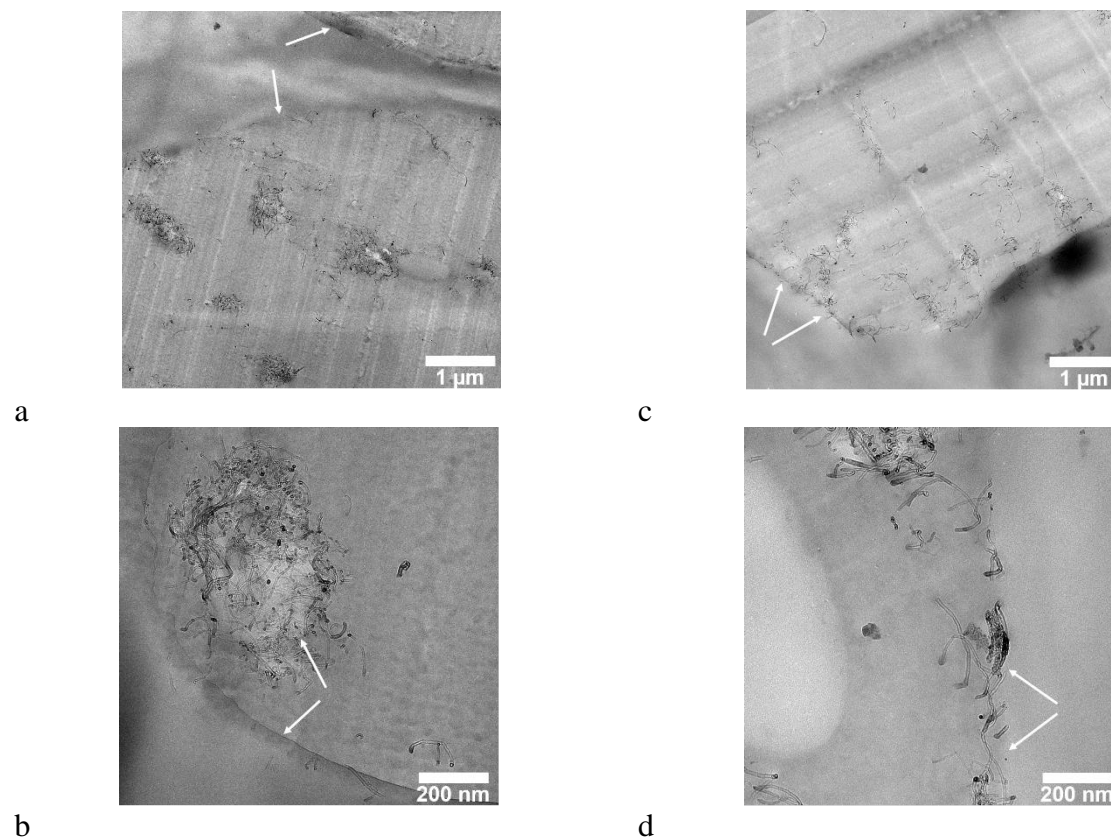


Figure 8. TEM of PP/PS/MWCNT composite with 0.5 wt.% of MWCNT for a-b) before treatment and c-d) after thermal annealing. Arrows show PP/PS interface.

Figure 7(b) shows the evolution of the storage modulus during thermal annealing. In this case, the power-law fitting of experimental data is presented. The fitted storage modulus (G') was normalized by its initial value ($G'_{initial}$) which was taken at the beginning of the test. The experimental values of G' were fluctuating during the early stage of thermal annealing (~10 min) (as shown in Figure S4 of the supplementary material), after that, G' values were slightly increasing and then approaching a plateau for filled PP/PS/MWCNT composites. However, in the case of neat PP/PS blend, G' was decreasing drastically during the first 10 min and then approaching a plateau. This behavior can be clearly seen in normalized fitted data.

In order to understand these changes in electrical conductivity and evolution of the storage moduli during thermal annealing, for the PP/PS/MWCNT composites, the SAOS experiments before and after thermal annealing were analyzed. The YZZ model (Equation (6)) was used for the systems containing less than 0.3 wt.% MWCNT. The modified YZZ model (Equation (9)) was used for the systems containing higher concentrations of MWCNT to characterize the morphologies of the blend before and after thermal annealing.

The values predicted by the YZZ model and the modified YZZ model are reported in Table 2. These values were used to calculate the characteristic domain size for each PP/PS/MWCNT composite before and after thermal annealing as shown in Figure 9.

Table 2. Fitting parameters for Equation (6) and Equation (9)

MWCNT, wt.%	G'_0 , Pa, before annealing	G'_0 , Pa, after annealing	a , μm , before annealing	a , μm , after annealing
0	-	-	4.95	7.67
0.1	-	-	1.96	1.67
0.3	66	74	1.18	0.91
0.5	124	158	0.85	0.69
1	257	389	0.65	0.53
2	1548	1677	0.59	0.42

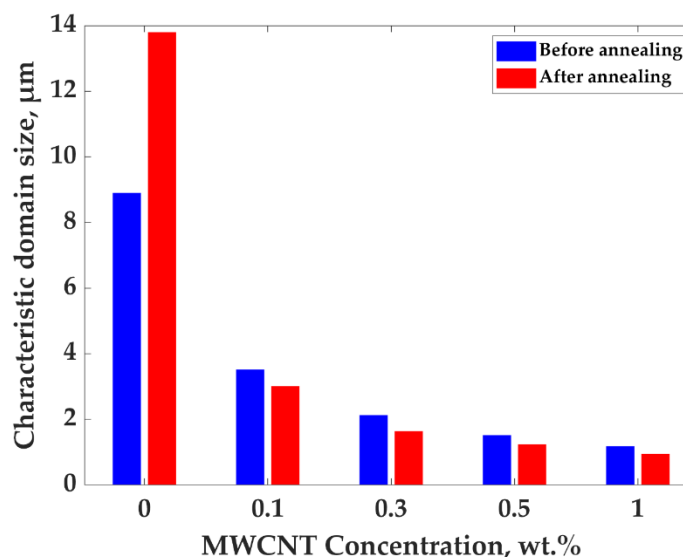


Figure 9. Characteristic domain size of PP/PS/MWCNT composites before and after 30 min of annealing calculated with the help of the YZZ model for PP/PS/MWCNT with 0-0.1 wt.% of MWCNT and the Equation (6) for PP/PS/MWCNT with 0.3-0.5 wt.% of MWCNT.

It can be seen, from Figure 9, that the characteristic domain size increased from 8.9 to 13.8 μm after 30 min of thermal annealing, for the neat PP/PS blend, indicating a blend morphology' coarsening [6,42]. Interestingly, for composites containing MWCNT, the characteristic domain size slightly decreased after 30 min of thermal annealing. This could indicate that migration of MWCNT from the PP to the more favorable PS prevented its coalescence and coarsening. This resulted in a more refined co-continuous morphology.

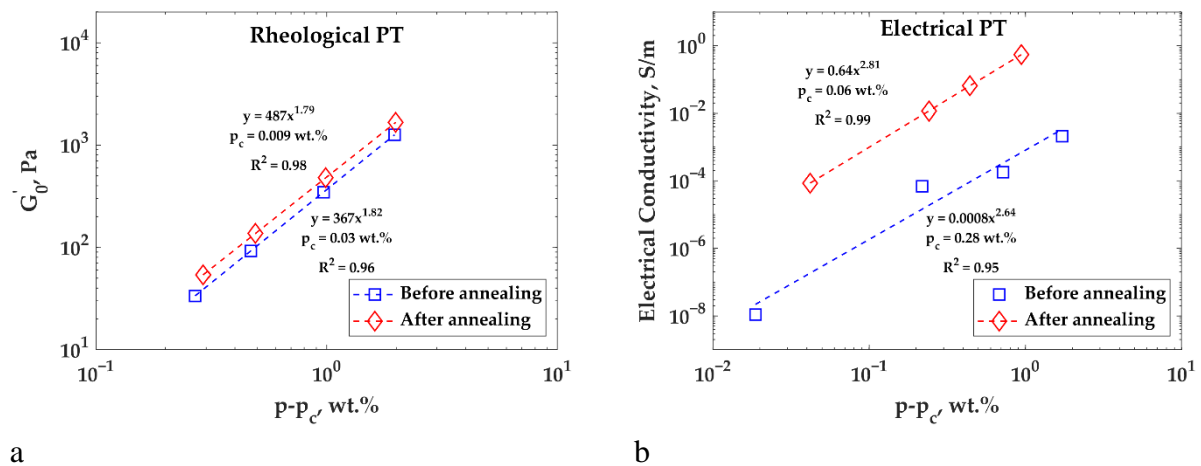
Data presented in Table 2 can help with further investigation of the elastic response mechanism in PP/PS/MWCNT composites, and in the estimation of the contribution of the filler network formation after thermal annealing. As was mentioned above, values of G'_0 for filled composites are constant at low-frequencies. These values can be used to estimate the rheological percolation threshold defined as the minimum particle concentration needed for the formation of a filler network as [36]:

$$G'_0 = k \cdot (p - p_c)^v \quad (10)$$

where G'_0 is frequency-independent elastic modulus, p is the mass fraction of MWCNT, p_c is the percolation threshold, v is a fitted exponent that depends, only, on the dimensionality of the

system, and k is a scaling factor responsible for strength of the filler network. It should be noted that this equation is valid for $p > p_c$.

A linear regression of $\log(G'_0)$ vs. $\log(p - p_c)$ was used to determine the rheological percolation threshold of the blends, studied in this work. The same calculations were done for the electrical conductivity before and after thermal annealing to determine the electrical percolation threshold. The experimental data for PP/PS/MWCNT composites before and after thermal annealing were fitted to equation (10) and the results are presented in Figure 10 for both the rheological (Figure 10(a)) and the electrical (Figure 10(b)) percolation thresholds (where values of σ' instead of G'_0 were used for calculation of electrical PT). Both rheological and electrical percolation threshold were decreased by thermal annealing: from 0.03 wt.% to 0.009 wt.% of MWCNT for rheological PT, and from 0.28 wt.% to 0.06 wt.% of MWCNT for electrical PT. It can be seen that rheological PT is smaller than the electrical one. This could indicate that adding a rigid filler to the polymer matrix can impede the movement of the polymer chains even at an ultra-low MWCNT concentration, due to the strong interaction between the filler and the polymer chains. However, in the case of the electrical conductivity, MWCNT-MWCNT contacts have to be dominant for easier charge transfer [48]. Therefore, the electrical PT is higher than the rheological one. It is worth noting that the stiffness of the network for both rheological and electrical PT is higher then that after thermal annealing. Rheological PT was found to be 367 Pa before compared to 487 Pa after thermal annealing. Similarly, electrical PT increased from $8 \cdot 10^{-4}$ S/m before to $6.4 \cdot 10^{-1}$ S/m after thermal annealing. This is attributed to the increase in the fraction of MWCNT located at the PP/PS interface after thermal annealing. The same behavior was observed for LLDPE/EVA co-continuous polymer blend containing graphene [10].



a b
Figure 10. Network elasticity as a function of reduced filler content related to PP/PS/MWCNT composites (solid squares) and power-law fitting to the experimental data (solid lines) for composites before and after thermal annealing: a) rheological PT – G'_0 vs. $(p - p_c)$ plots and b) electrical PT σ' vs. $(p - p_c)$ plots

IV. CONCLUSION

In this study, the linear viscoelastic behavior of a co-continuous PP/PS blend containing an electrically conductive filler – MWCNT was investigated. PP/PS/MWCNT composites were prepared by melt-mixing, using a twin-screw extruder by the dilution of a masterbatch of PP/MWCNT with PP and PS. The linear viscoelastic behavior of PP/PS/MWCNT composites was investigated by the YZZ model. It was shown that this model fails to describe the rheological behaviour of highly filled composites at lower frequencies. The discrepancy between the experimental values of the storage modulus and the one predicted by the YZZ model, due to a significant contribution of filler network elasticity to the dynamic modulus. To consider this contribution, a modified YZZ model is proposed in this work for PP/PS/MWCNT composites. By using the modified YZZ model it was possible to quantify the co-continuous morphology of PP/PS/MWCNT composites. It was shown that a good agreement between the characteristic domain size, predicted by this model and that calculated via statistical analysis of SEM images was achieved. Furthermore, the modified YZZ model was used to study the evolution of the co-continuous morphology of PP/PS/MWCNT composites after thermal annealing. It was observed that the characteristic domain size, calculated with the modified YZZ model, slightly decreased after 30 min of thermal annealing. This resulted in a more refined co-continuous morphology. This is in good agreement with the measured electrical properties of these composites. It was shown that the electrical percolation threshold was reduced by over 70% as a result of thermal annealing.

SUPPLEMENTARY MATERIAL

See supplementary material for the additional information of experimental data: storage and loss moduli as a function of frequency for PP/PS/MWCNT composites with different concentrations of MWCNT. The model fitting data; SEM image treatment analysis; time-dependent evolution of storage modulus; and electrical conductivity as a function of time for PP/PS/MWCNT and PP/MWCNT composites.

ACKNOWLEDGMENTS

Financial supports from the Natural Sciences and Engineering Research Council of Canada (NSERC), PRIMA, and École de technologie supérieure (ÉTS) are gratefully acknowledged. The help of Mr. Mazen Samara in reviewing English is highly appreciated.

REFERENCES

1. Yu, W.; Zhou, W.; Zhou, C. Linear viscoelasticity of polymer blends with co-continuous morphology. *Polymer* **2010**, *51*, 2091-2098.
2. Sadeghi, S.; Arjmand, M.; Otero Navas, I.; Zehtab Yazdi, A.; Sundararaj, U. Effect of nanofiller geometry on network formation in polymeric nanocomposites: Comparison of rheological and electrical properties of multiwalled carbon nanotube and graphene nanoribbon. *Macromolecules* **2017**, *50*, 3954-3967.
3. Otero-Navas, I.; Arjmand, M.; Sundararaj, U. Carbon nanotube induced double percolation in polymer blends: Morphology, rheology and broadband dielectric properties. *Polymer* **2017**, *114*, 122-134.

4. Helal, E.; Amurin, L.; Carastan, D.; de Sousa Jr, R.; David, E.; Frechette, M.; Demarquette, N. Interfacial molecular dynamics of styrenic block copolymer-based nanocomposites with controlled spatial distribution. *Polymer* **2017**, *113*, 9-26.
5. Trifkovic, M.; Hedegaard, A.T.; Sheikhzadeh, M.; Huang, S.; Macosko, C.W. Stabilization of PE/PEO cocontinuous blends by interfacial nanoclays. *Macromolecules* **2015**, *48*, 4631-4644.
6. Bai, L.; He, S.; Fruehwirth, J.W.; Stein, A.; Macosko, C.W.; Cheng, X. Localizing graphene at the interface of cocontinuous polymer blends: Morphology, rheology, and conductivity of cocontinuous conductive polymer composites. *J Rheol* **2017**, *61*, 575-587.
7. Kuester, S.; Demarquette, N.R.; Ferreira Jr, J.C.; Soares, B.G.; Barra, G.M. Hybrid nanocomposites of thermoplastic elastomer and carbon nanoadditives for electromagnetic shielding. *Eur Polym J* **2017**, *88*, 328-339.
8. Kuester, S.; Barra, G.M.; Ferreira Jr, J.C.; Soares, B.G.; Demarquette, N.R. Electromagnetic interference shielding and electrical properties of nanocomposites based on poly (styrene-*b*-ethylene-ran-butylene-*b*-styrene) and carbon nanotubes. *Eur Polym J* **2016**, *77*, 43-53.
9. Strugova, D.; Ferreira Junior, J.C.; David, É.; Demarquette, N.R. Ultra-Low Percolation Threshold Induced by Thermal Treatments in Co-Continuous Blend-Based PP/PS/MWCNTs Nanocomposites. *Nanomaterials-Basel* **2021**, *11*, 1620.
10. Helal, E.; Kurusu, R.S.; Moghimian, N.; Gutierrez, G.; David, E.; Demarquette, N.R. Correlation between morphology, rheological behavior, and electrical behavior of conductive cocontinuous LLDPE/EVA blends containing commercial graphene nanoplatelets. *J Rheol* **2019**, *63*, 961-976.
11. Kurusu, R.S.; Helal, E.; Moghimian, N.; David, E.; Demarquette, N. The role of selectively located commercial graphene nanoplatelets in the electrical properties, morphology, and stability of EVA/LLDPE blends. *Macromolecular Materials and Engineering* **2018**, *303*, 1800187.
12. Chen, Y.; Yang, Q.; Huang, Y.; Liao, X.; Niu, Y. Influence of phase coarsening and filler agglomeration on electrical and rheological properties of MWNTs-filled PP/PMMA composites under annealing. *Polymer* **2015**, *79*, 159-170.
13. Huang, J.; Mao, C.; Zhu, Y.; Jiang, W.; Yang, X. Control of carbon nanotubes at the interface of a co-continuous immiscible polymer blend to fabricate conductive composites with ultralow percolation thresholds. *Carbon* **2014**, *73*, 267-274.
14. Genoyer, J.; Demarquette, N.R.; Soulestin, J. Effect of clay particles size and location on coalescence in PMMA/PS blends. *J Rheol* **2019**, *63*, 883-893.
15. Genoyer, J.; Soulestin, J.; Demarquette, N.R. Influence of the molar masses on compatibilization mechanism induced by two block copolymers in PMMA/PS blends. *J Rheol* **2018**, *62*, 681-693.
16. Paliarne, J. Linear rheology of viscoelastic emulsions with interfacial tension. *Rheol Acta* **1990**, *29*, 204-214.
17. Gramespacher, H.; Meissner, J. Interfacial tension between polymer melts measured by shear oscillations of their blends. *J Rheol* **1992**, *36*, 1127-1141.
18. Bousmina, M. Effect of interfacial tension on linear viscoelastic behavior of immiscible polymer blends. *Rheol Acta* **1999**, *38*, 251-254.
19. Souza, A.M.C.d.; Calvao, P.S.; Demarquette, N.R. Linear viscoelastic behavior of compatibilized PMMA/PP blends. *J Appl Polym Sci* **2013**, *129*, 1280-1289.

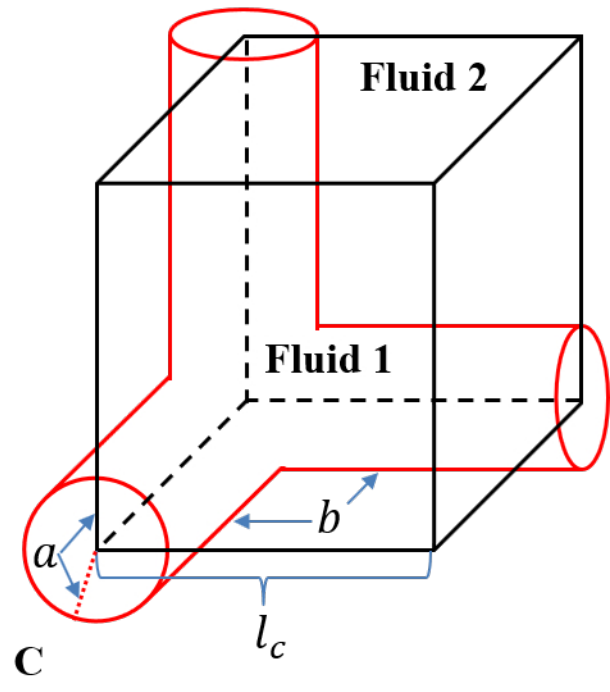
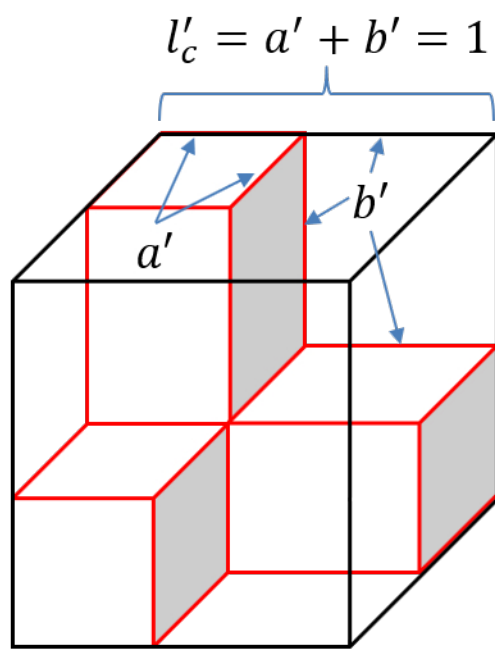
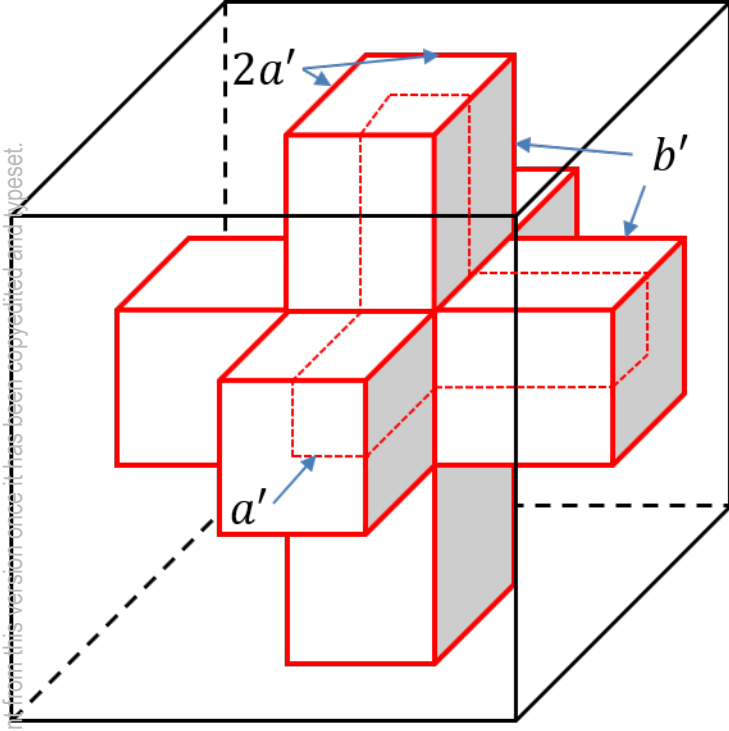
This is the author's peer reviewed, accepted manuscript. However, the online version of record will be different from this version once it has been copyedited and typeset.
PLEASE CITE THIS ARTICLE AS DOI: 10.1122/1.5000044

20. Bose, S.; Bhattacharyya, A.R.; Kulkarni, A.R.; Pötschke, P. Electrical, rheological and morphological studies in co-continuous blends of polyamide 6 and acrylonitrile–butadiene–styrene with multiwall carbon nanotubes prepared by melt blending. *Compos Sci Technol* **2009**, *69*, 365-372.
21. Scherzer, S.L.; Pavlova, E.; Esper, J.D.; Starý, Z. Phase structure, rheology and electrical conductivity of co-continuous polystyrene/polymethylmethacrylate blends filled with carbon black. *Compos Sci Technol* **2015**, *119*, 138-147.
22. Omonov, T.; Harrats, C.; Moldenaers, P.; Groeninckx, G. Phase continuity detection and phase inversion phenomena in immiscible polypropylene/polystyrene blends with different viscosity ratios. *Polymer* **2007**, *48*, 5917-5927.
23. Vandebril, S.; Vermant, J.; Moldenaers, P. Efficiently suppressing coalescence in polymer blends using nanoparticles: role of interfacial rheology. *Soft Matter* **2010**, *6*, 3353-3362.
24. Thareja, P.; Moritz, K.; Velankar, S.S. Interfacially active particles in droplet/matrix blends of model immiscible homopolymers: Particles can increase or decrease drop size. *Rheol Acta* **2010**, *49*, 285-298.
25. Thareja, P.; Velankar, S. Rheology of immiscible blends with particle-induced drop clusters. *Rheol Acta* **2008**, *47*, 189-200.
26. Vermant, J.; Cioccolo, G.; Nair, K.G.; Moldenaers, P. Coalescence suppression in model immiscible polymer blends by nano-sized colloidal particles. *Rheol Acta* **2004**, *43*, 529-538.
27. Bose, S.; Ozdilek, C.; Leys, J.; Seo, J.W.; Wübbenhorst, M.; Vermant, J.; Moldenaers, P. Phase separation as a tool to control dispersion of multiwall carbon nanotubes in polymeric blends. *Acs Appl Mater Inter* **2010**, *2*, 800-807.
28. Charfeddine, I.; Majesté, J.; Carrot, C.; Lhost, O. A model for the prediction of the morphology of immiscible blends of polymers. *Polymer* **2020**, *193*, 122334.
29. Sengers, W.; Sengupta, P.; Noordermeer, J.W.; Picken, S.; Gotsis, A. Linear viscoelastic properties of olefinic thermoplastic elastomer blends: melt state properties. *Polymer* **2004**, *45*, 8881-8891.
30. Vinckier, I.; Laun, H. Assessment of the Doi–Ohta theory for co-continuous blends under oscillatory flow. *J Rheol* **2001**, *45*, 1373-1385.
31. Coran, A.; Patel, R. Predicting elastic moduli of heterogeneous polymer compositions. *J Appl Polym Sci* **1976**, *20*, 3005-3016.
32. Huang, C.; Yu, W. Role of block copolymer on the coarsening of morphology in polymer blend: effect of micelles. *AIChE Journal* **2015**, *61*, 285-295.
33. Veenstra, H.; Verkooijen, P.C.; van Lent, B.J.; van Dam, J.; de Boer, A.P.; Nijhof, A.P.H. On the mechanical properties of co-continuous polymer blends: experimental and modelling. *Polymer* **2000**, *41*, 1817-1826.
34. Chen, J.; Liao, X.; Li, S.; Wang, W.; Guo, F.; Li, G. A promising strategy for efficient electromagnetic interference shielding by designing a porous double-percolated structure in MWCNT/polymer-based composites. *Composites Part A: Applied Science and Manufacturing* **2020**, *138*, 106059.
35. Jordhamo, G.; Manson, J.; Sperling, L. Phase continuity and inversion in polymer blends and simultaneous interpenetrating networks. *Polymer Engineering & Science* **1986**, *26*, 517-524.
36. Filippone, G.; Salzano de Luna, M. A unifying approach for the linear viscoelasticity of polymer nanocomposites. *Macromolecules* **2012**, *45*, 8853-8860.

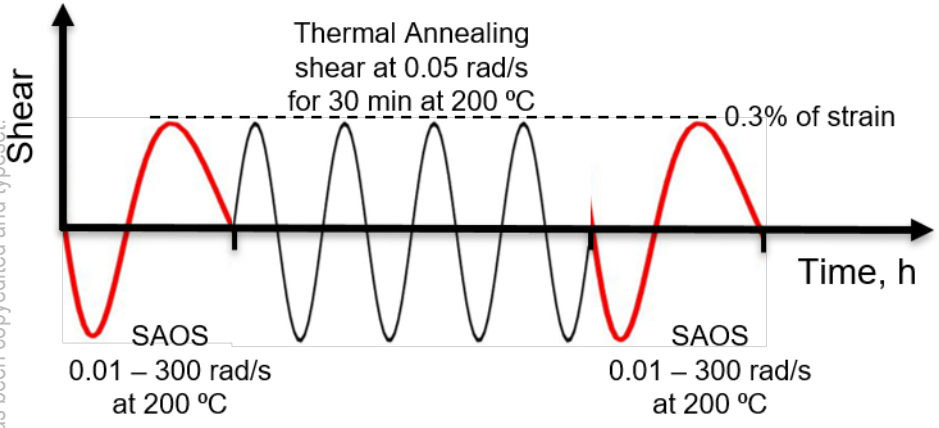
This is the author's peer reviewed, accepted manuscript. However, the online version of record will be different from this version once it has been copyedited and typeset.
PLEASE CITE THIS ARTICLE AS DOI: 10.1122/1.5000044

37. Filippone, G.; Causa, A.; de Luna, M.S.; Sanguigno, L.; Acierno, D. Assembly of plate-like nanoparticles in immiscible polymer blends—effect of the presence of a preferred liquid–liquid interface. *Soft Matter* **2014**, *10*, 3183-3191.
38. Altobelli, R.; de Luna, M.S.; Filippone, G. Interfacial crowding of nanoplatelets in co-continuous polymer blends: Assembly, elasticity and structure of the interfacial nanoparticle network. *Soft Matter* **2017**, *13*, 6465-6473.
39. Bird, R.B.; Armstrong, R.C.; Hassager, O. Dynamics of polymeric liquids. Vol. 1: Fluid mechanics. **1987**.
40. Carreau, P.J.; De Kee, D.C.; Chhabra, R.P. *Rheology of polymeric systems: principles and applications*; Carl Hanser Verlag GmbH Co KG: 2021.
41. Macaubas, P.; Demarquette, N. Morphologies and interfacial tensions of immiscible polypropylene/polystyrene blends modified with triblock copolymers. *Polymer* **2001**, *42*, 2543-2554.
42. Bai, L.; Sharma, R.; Cheng, X.; Macosko, C.W. Kinetic control of graphene localization in co-continuous polymer blends via melt compounding. *Langmuir* **2018**, *34*, 1073-1083.
43. Galloway, J.A.; Montminy, M.D.; Macosko, C.W. Image analysis for interfacial area and cocontinuity detection in polymer blends. *Polymer* **2002**, *43*, 4715-4722.
44. Pawar, S.P.; Bose, S. Peculiar morphological transitions induced by nanoparticles in polymeric blends: retarded relaxation or altered interfacial tension? *Phys Chem Chem Phys* **2015**, *17*, 14470-14478.
45. Bharati, A.; Cardinaels, R.; Seo, J.W.; Wübberhorst, M.; Moldenaers, P. Enhancing the conductivity of carbon nanotube filled blends by tuning their phase separated morphology with a copolymer. *Polymer* **2015**, *79*, 271-282.
46. Nasti, G.; Gentile, G.; Cerruti, P.; Carfagna, C.; Ambrogi, V. Double percolation of multiwalled carbon nanotubes in polystyrene/polylactic acid blends. *Polymer* **2016**, *99*, 193-203.
47. Alig, I.; Skipa, T.; Lellinger, D.; Pötschke, P. Destruction and formation of a carbon nanotube network in polymer melts: Rheology and conductivity spectroscopy. *Polymer* **2008**, *49*, 3524-3532.
48. Alig, I.; Pötschke, P.; Lellinger, D.; Skipa, T.; Pegel, S.; Kasaliwal, G.R.; Villmow, T. Establishment, morphology and properties of carbon nanotube networks in polymer melts. *Polymer* **2012**, *53*, 4-28.

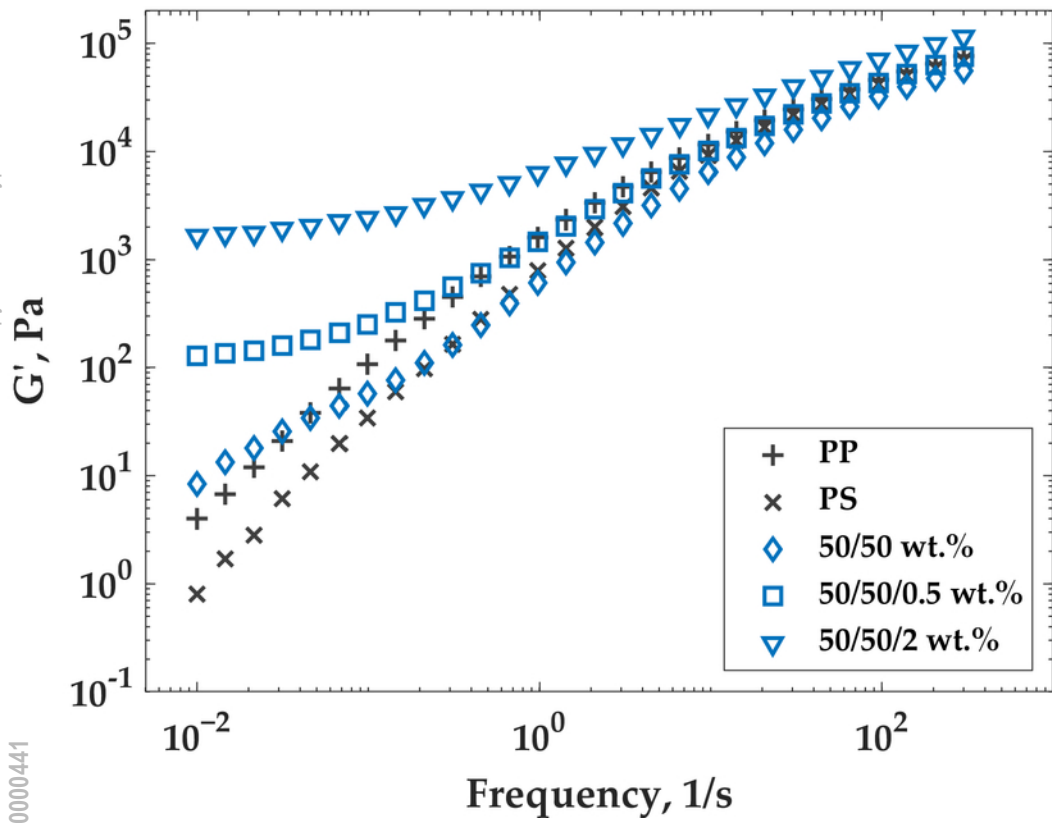
This is the author's peer reviewed, accepted manuscript. However, the online version of record will be different from this version once it has been copyedited and typeset.
PLEASE CITE THIS ARTICLE AS DOI: 10.1122/8.0000444



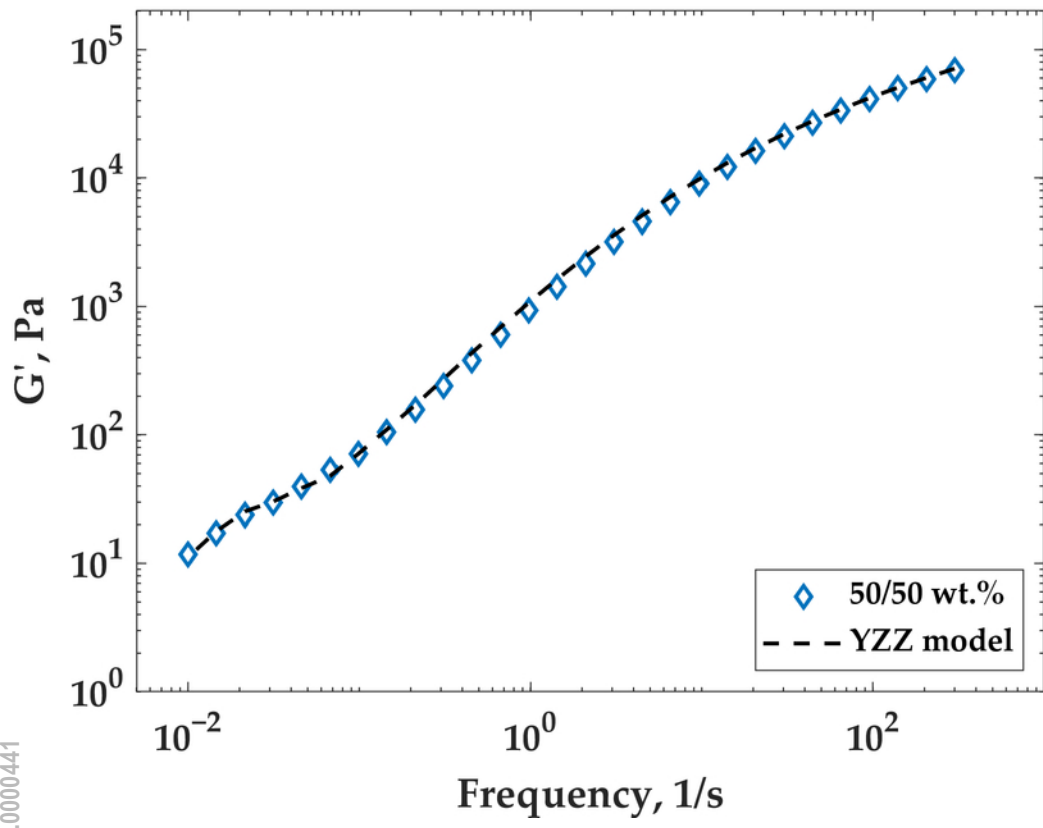
This is the author's peer reviewed, accepted manuscript. However, the online version of record will be different from this version once it has been copyedited and typeset.
PLEASE CITE THIS ARTICLE AS DOI: 10.1122/8.0000441



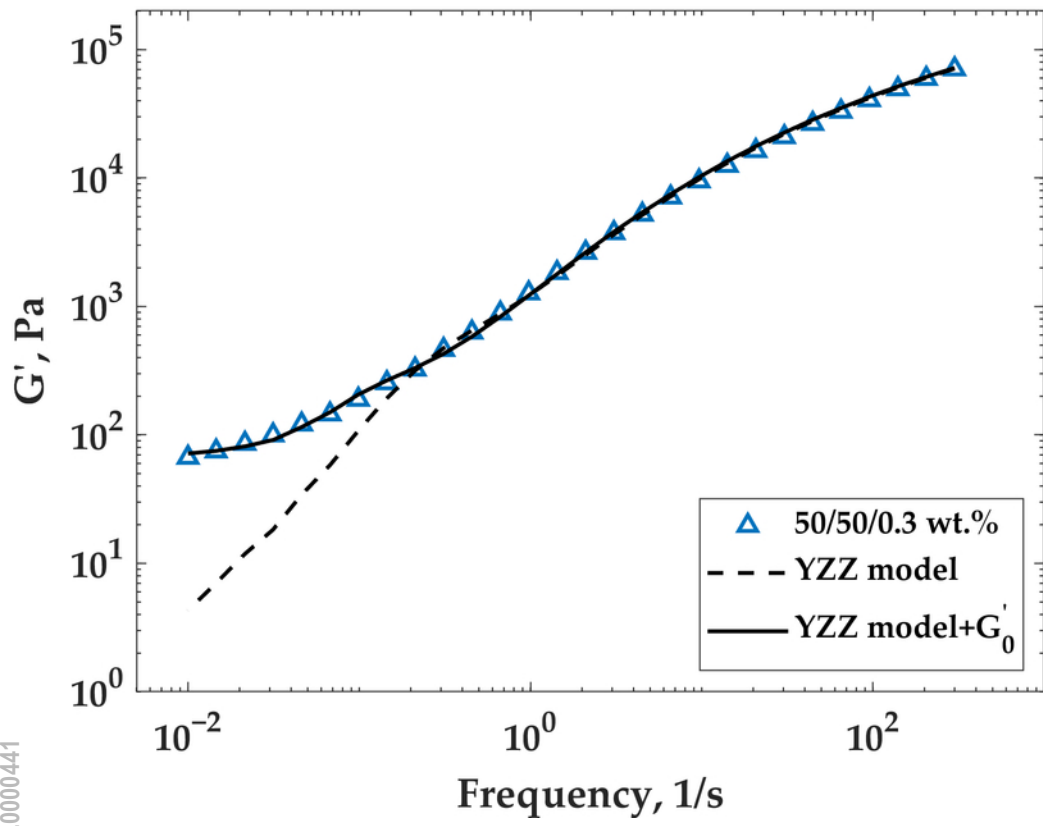
This is the author's peer reviewed, accepted manuscript. However, the online version of record will be different from this version once it has been copyedited and typeset.
 PLEASE CITE THIS ARTICLE AS DOI: 10.1122/8.0000441



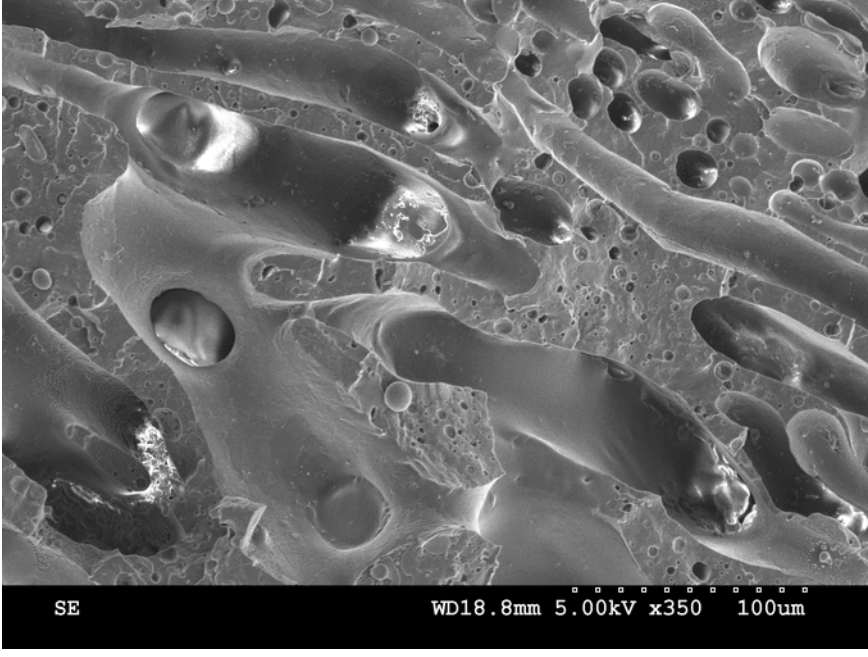
This is the author's peer reviewed, accepted manuscript. However, the online version of record will be different from this version once it has been copyedited and typeset.
PLEASE CITE THIS ARTICLE AS DOI: 10.1122/8.0000441



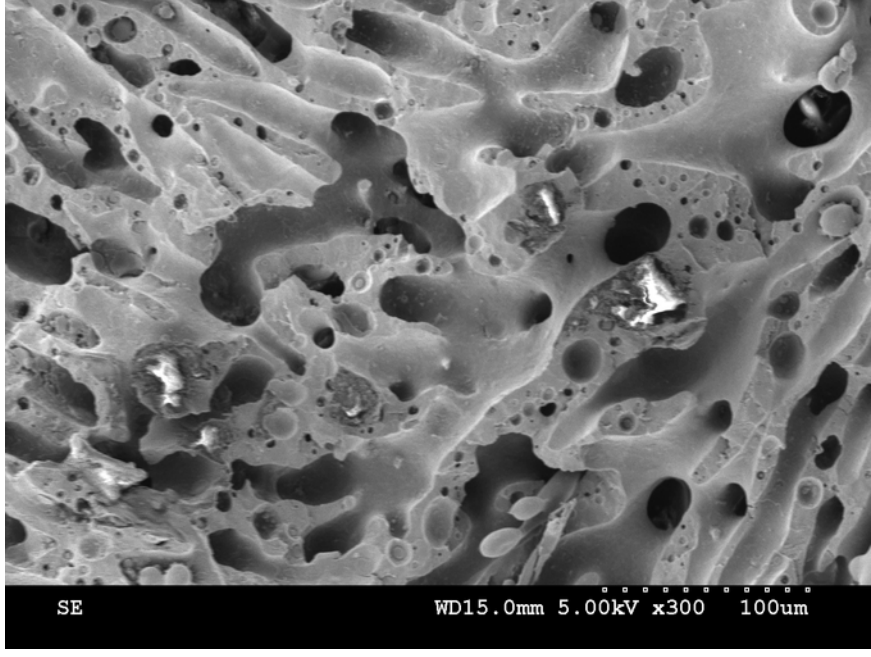
This is the author's peer reviewed, accepted manuscript. However, the online version of record will be different from this version once it has been copyedited and typeset.
PLEASE CITE THIS ARTICLE AS DOI: 10.1122/8.0000441



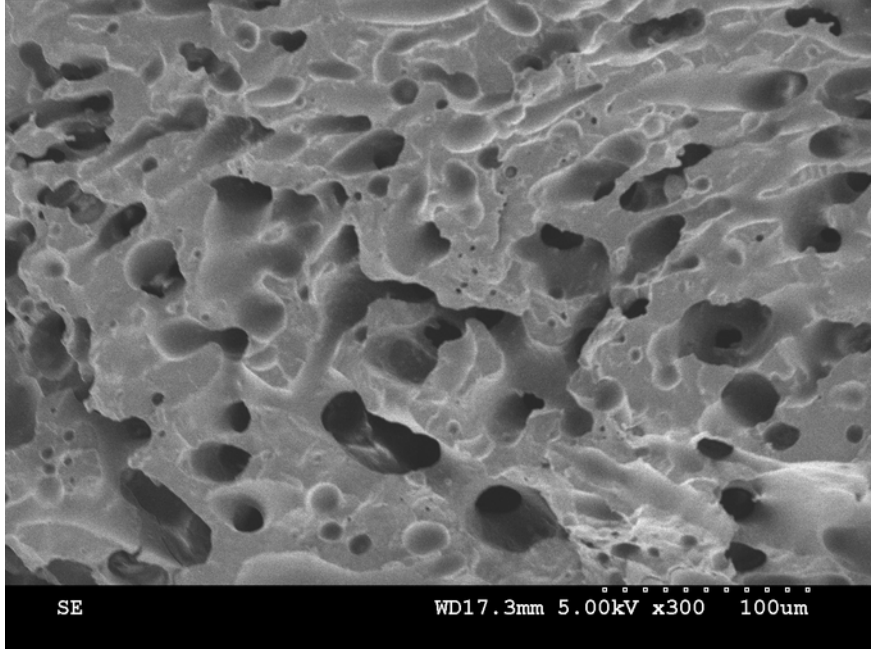
This is the author's peer reviewed, accepted manuscript. However, the online version of record will be different from this version once it has been copyedited and typeset.
PLEASE CITE THIS ARTICLE AS DOI: 10.1122/8.0000441



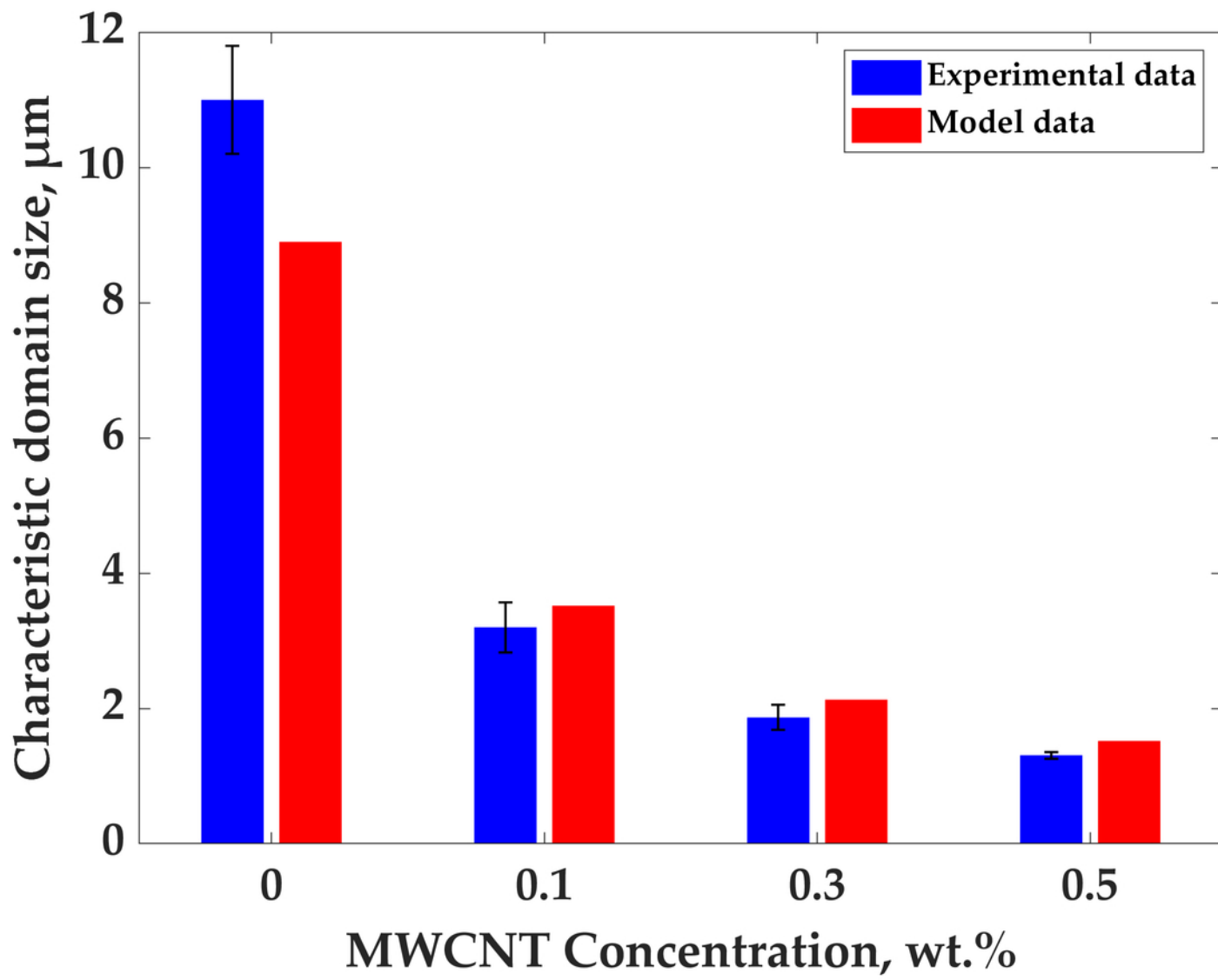
This is the author's peer reviewed, accepted manuscript. However, the online version of record will be different from this version once it has been copyedited and typeset.
PLEASE CITE THIS ARTICLE AS DOI: 10.1122/8.0000441



This is the author's peer reviewed, accepted manuscript. However, the online version of record will be different from this version once it has been copyedited and typeset.
PLEASE CITE THIS ARTICLE AS DOI: 10.1122/8.0000441

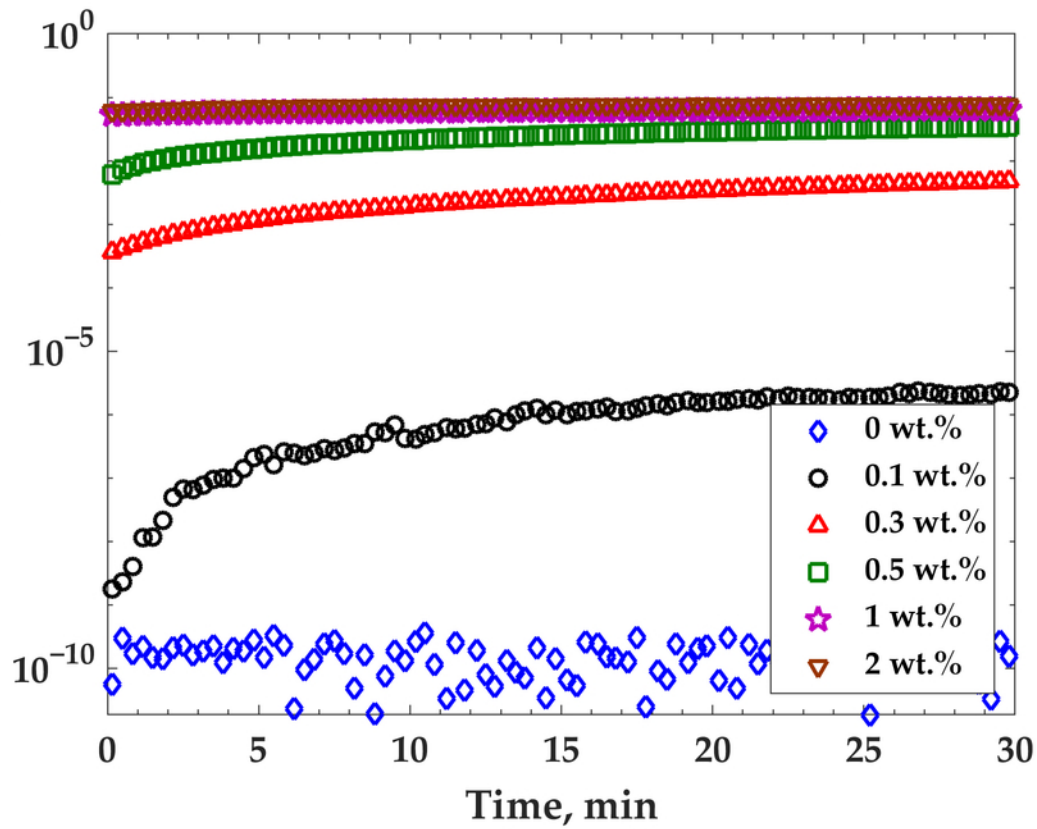


This is the author's peer reviewed, accepted manuscript. However, the online version of record will be different from this version once it has been copyedited and typeset.
 PLEASE CITE THIS ARTICLE AS DOI: 10.1122/8.0000441

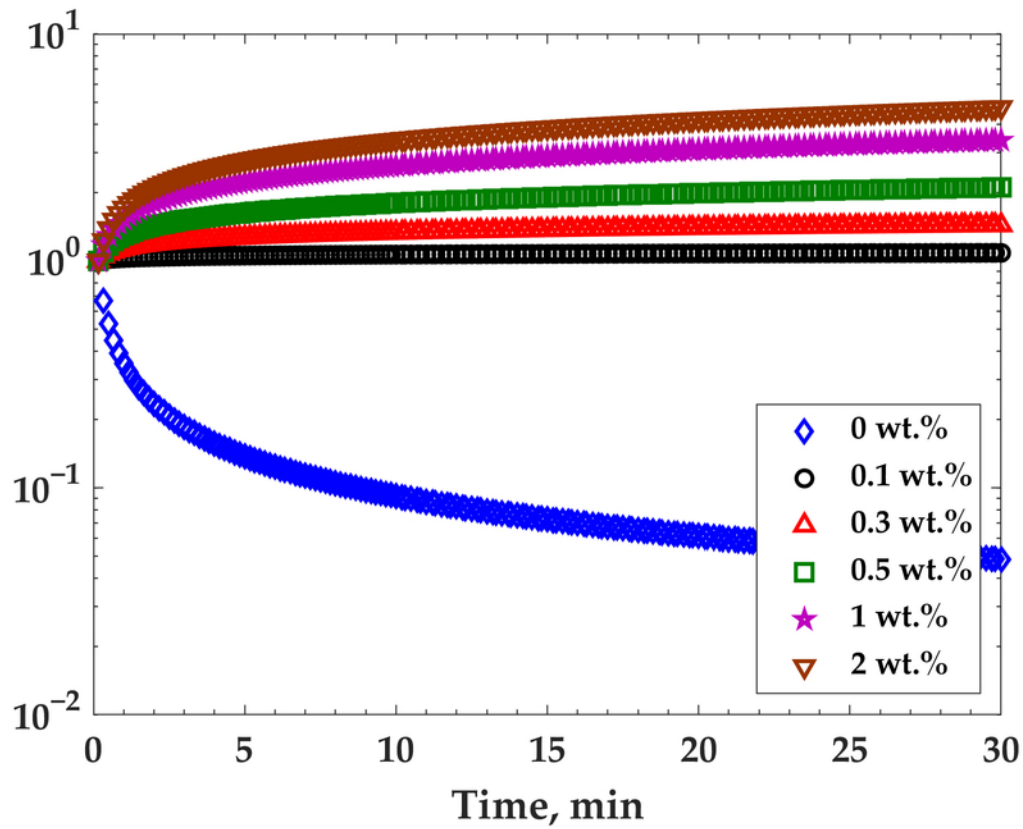


This is the author's peer reviewed, accepted manuscript. However, the online version of record will be different from this version once it has been copyedited and typeset.
 PLEASE CITE THIS ARTICLE AS DOI: 10.1122/8.0000441

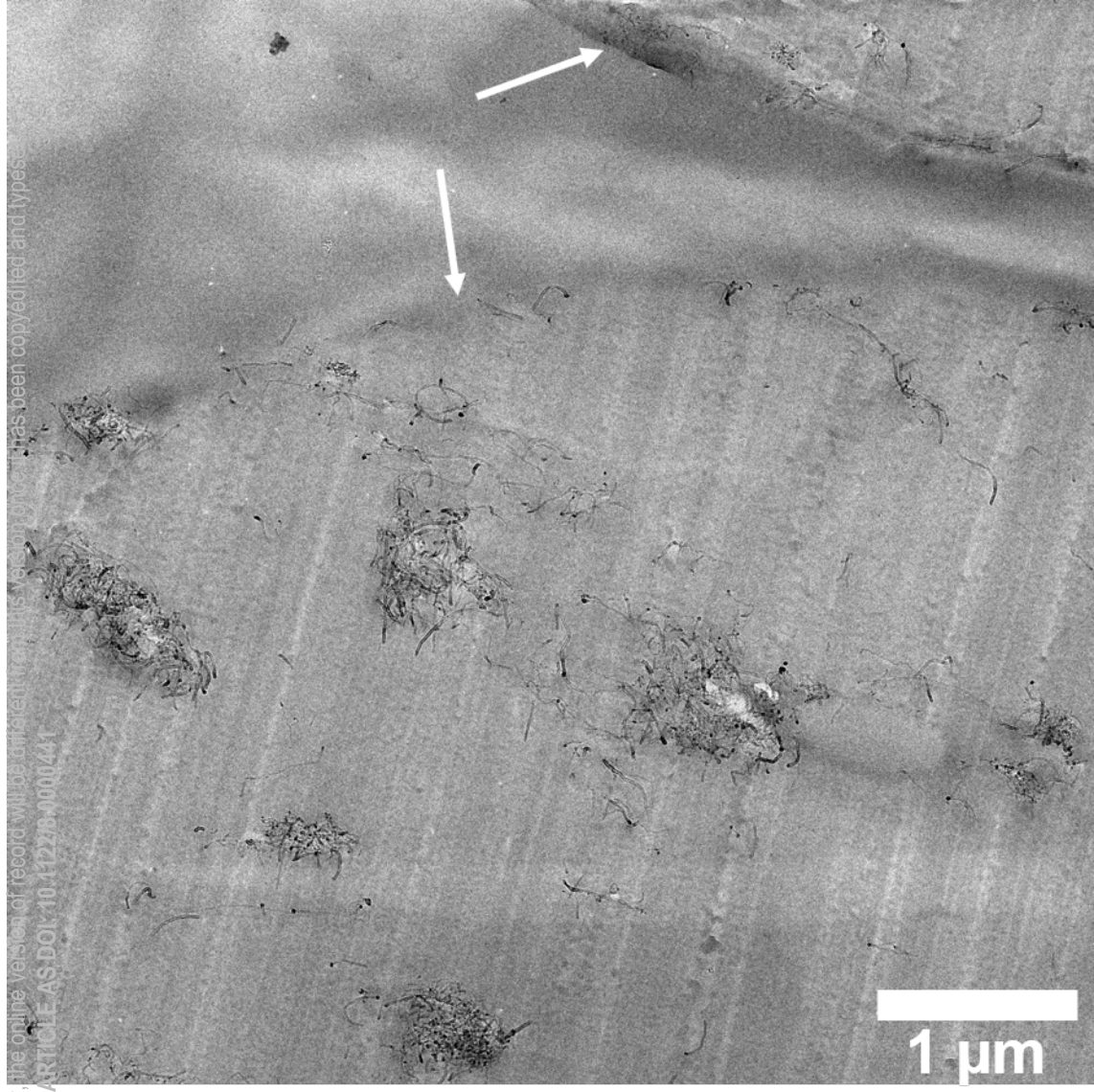
Electrical Conductivity, S/m



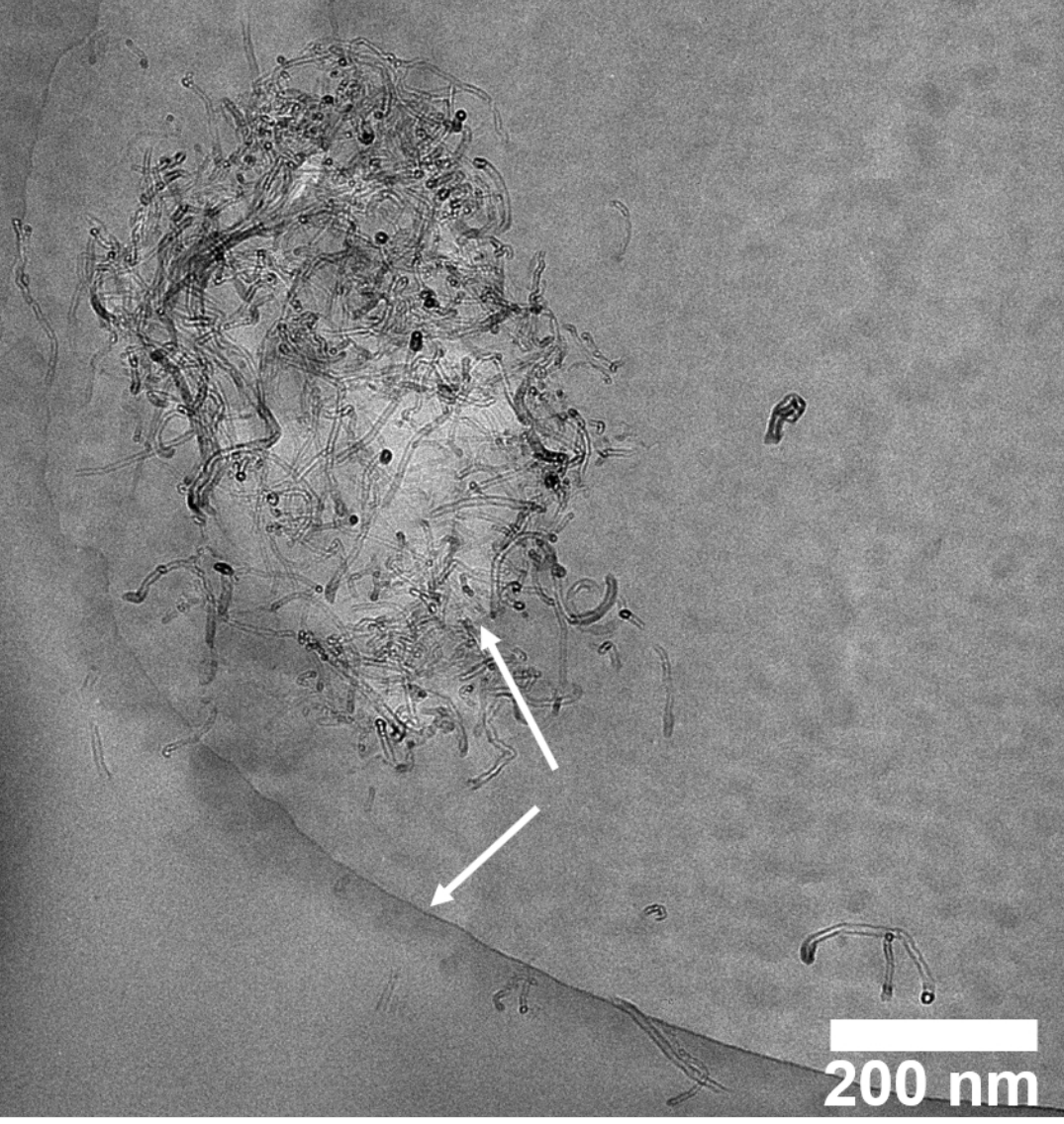
This is the author's peer reviewed, accepted manuscript. However, the online version of record will be different from this version once it has been copyedited and typeset.
PLEASE CITE THIS ARTICLE AS DOI: 10.1122/8.0000441



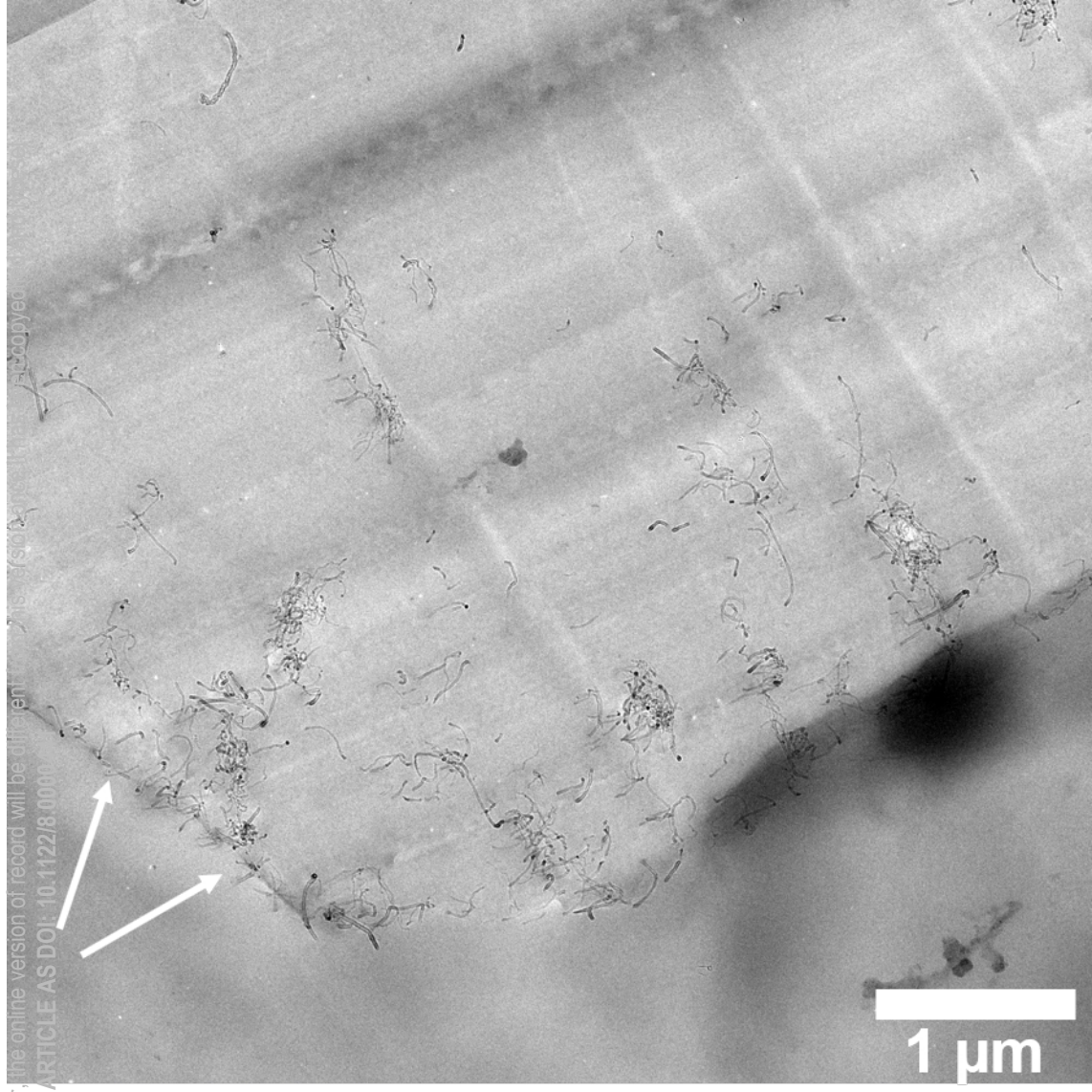
This is the author's peer reviewed, accepted manuscript. However, the online version of record will be different from this version because it has been copyedited and typeset. PLEASE CITE THIS ARTICLE AS DOI: 10.1122/JRR-2020-0000441



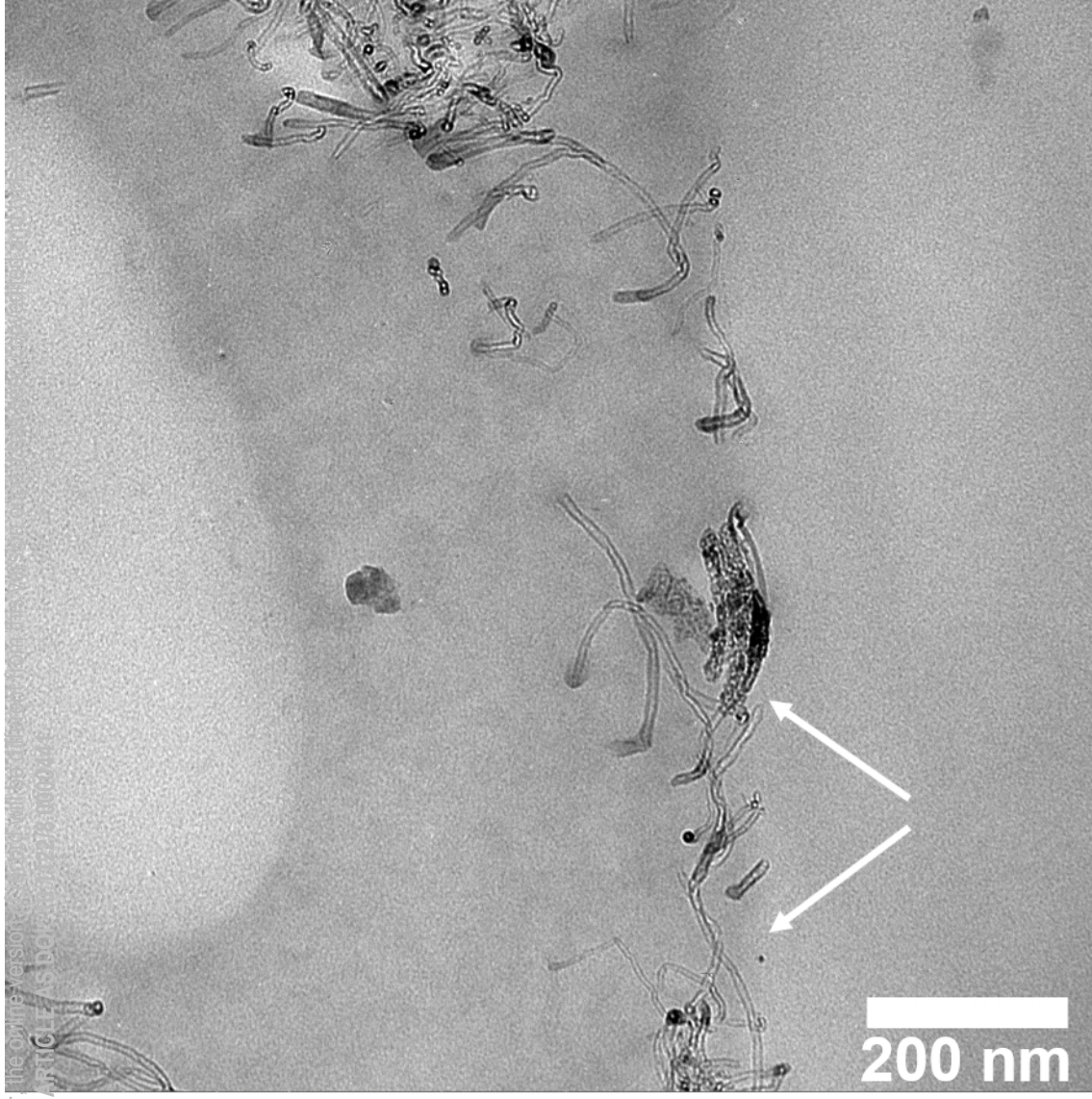
This is the author's peer reviewed, accepted manuscript. However, the online version of record will be different from this version once it has been copyedited and typeset.
PLEASE CITE THIS ARTICLE AS DOI: 10.1122/8.0000441



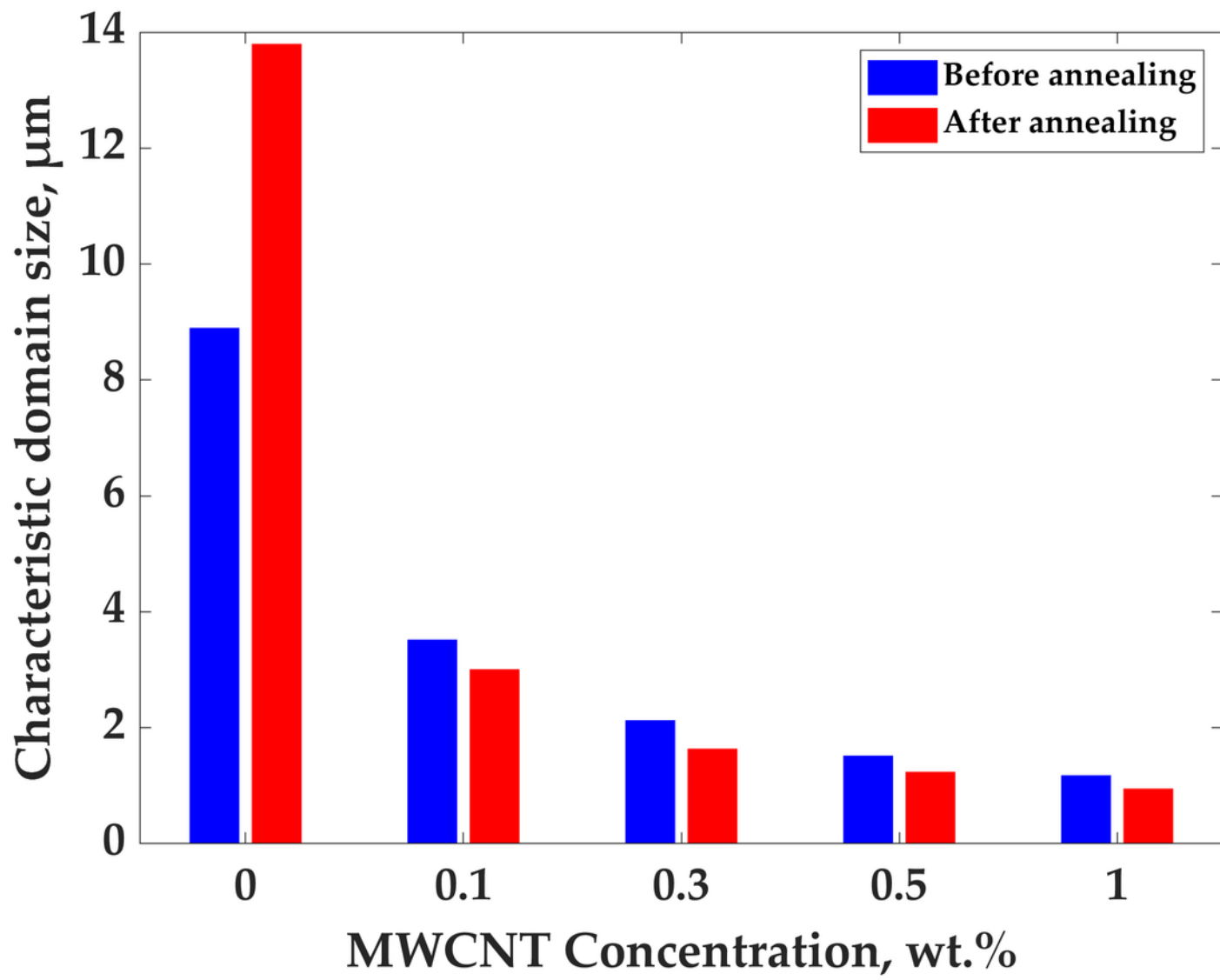
This is the author's peer reviewed, accepted manuscript. However, the online version of record will be different from this version because the final published version may be edited, formatted, and proofread.
PLEASE CITE THIS ARTICLE AS DOI: 10.1122/1.8.0000



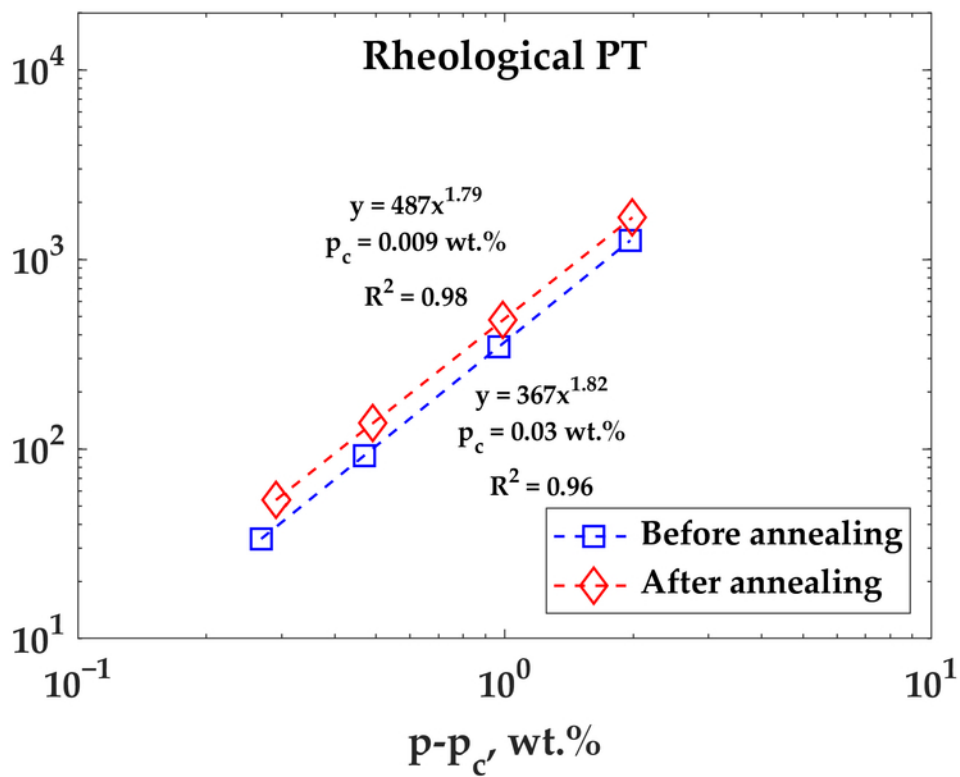
This is the author's peer reviewed, accepted manuscript. However, the online version of this article is not yet copyedited or proofread. Please cite this article as: <https://doi.org/10.1137/19M1100000>



This is the author's peer reviewed, accepted manuscript. However, the online version of record will be different from this version once it has been copyedited and typeset.
PLEASE CITE THIS ARTICLE AS DOI: 10.1122/8.0000441



This is the author's peer reviewed, accepted manuscript. However, the online version of record will be different from this version once it has been copyedited and typeset.
 PLEASE CITE THIS ARTICLE AS DOI: 10.1122/8.0000441



This is the author's peer reviewed, accepted manuscript. However, the online version of record will be different from this version once it has been copyedited and typeset.
PLEASE CITE THIS ARTICLE AS DOI: 10.1122/8.0000441

Electrical Conductivity, S/m

